Late Paleocene – early Eocene Arctic Ocean Sea Surface Temperatures: reassessing biomarker paleothermometry at Lomonosov Ridge

Appy Sluijs[1], Joost Frieling[1], Gordon N. Inglis[2 *], Klaas G.J. Nierop[1], Francien Peterse[1], Francesca Sangiorgi[1] and Stefan Schouten[1,3]

[1]Department of Earth Sciences, Faculty of Geosciences, Utrecht University. Princetonlaan 8a, 3584 CB Utrecht, The Netherlands

[2]Organic Geochemistry Unit, School of Chemistry, School of Earth Sciences, University of Bristol, Bristol, UK

[3]NIOZ Royal Institute for Sea Research, Department of Microbiology and Biogeochemistry, and Utrecht University, PO Box 59, 1790AB Den Burg, The Netherlands

[*] present address: School of Ocean and Earth Science, National Oceanography Centre Southampton, University of Southampton, UK

Abstract

A series of papers shortly following Integrated Ocean Drilling Program Arctic Coring Expedition (ACEX, 2004) on Lomonosov Ridge indicated remarkably high early Eocene sea surface temperatures (SST; ca. 23 to 27 °C) and land air temperatures (ca. 17 to 25 °C) based on the distribution of isoprenoid and branched glycerol dialkyl glycerol tetraether (isoGDGT and brGDGT) lipids, respectively. Here, we revisit these results using recent analytical developments – which have led to improved temperature calibrations and the discovery of new temperature-sensitive glycerol monoalkyl glycerol tetraethers (GMGTs) – and currently available proxy constraints.

The isoGDGT assemblages support temperature as the dominant variable controlling TEX_{86} values for most samples. However, contributions of isoGDGTs from land, which we characterize in detail, complicate TEX_{86} paleothermometry in the late Paleocene and part of the interval between the Paleocene-Eocene Thermal Maximum (PETM; ~56 Ma) and Eocene Thermal Maximum 2 (ETM2; ~54 Ma). Background early Eocene SSTs generally exceeded 20 °C, with peak warmth during the PETM (~26 °C) and ETM2 (~27 °C). We find abundant branched GMGTs, likely dominantly marine in origin, and their distribution responds to environmental change. Further modern work is required to test to what extent temperature and other environmental factors determine their distribution.

Published Arctic vegetation reconstructions indicate coldest month mean continental air temperatures of 6-13 °C, which reinforces the question if TEX_{86}-derived SSTs in the Paleogene Arctic are skewed towards the summer season. The exact meaning of TEX_{86} in the Paleogene Arctic thus remains a fundamental issue, and one that limits our assessment of the performance of fully-coupled climate models under greenhouse conditions.

1. Introduction

The Eocene epoch (56 to 34 million years ago; Ma) has long been characterized by warm climates. The earliest signs of a balmy Eocene Arctic region – fossil leaves of numerous plant species – were documented 150 years ago (Heer, 1869). Subsequent findings identified palms, baobab and mangroves, indicating the growth of temperate rainforests and year-round frost-free conditions in the Eocene Arctic region (Schweitzer, 1980; Greenwood and Wing, 1995; Suan et al., 2017; Willard et al., 2019). Fossils of animals, including varanid lizards, tortoises and alligators also indicate warm Arctic climates (Dawson et al., 1976; Estes and Hutchinson, 1980). These earliest findings sparked interest into the climatological mechanisms allowing for such polar warmth about a century ago (Berry, 1922). Ever since, paleobotanists have focused on the Arctic plant fossils and have significantly refined their paleoclimatological interpretation towards estimates of precipitation as well as seasonal and mean annual temperature (e.g. Uhl et al., 2007; Greenwood et al., 2010; Eberle and Greenwood, 2012; Suan et al., 2017; Willard et al., 2019).

Novel insights in Paleogene Arctic paleoclimate research were made in the years following the Arctic Coring Expedition 302 (ACEX, Integrated Ocean Drilling Program (IODP) 2004, Figure 1). This expedition recovered upper Paleocene and lower Eocene siliciclastic sediments, deposited in a shallow marine environment, in Hole 4A (87° 52.00 ‘N; 136° 10.64 ’E; 1,288 m water depth), on the Lomonosov Ridge in the central Arctic Ocean (Backman et al., 2006). The succession was deposited at a paleolatitude of ~78 °N, based on a geological reconstruction (Seton et al., 2012) projected using a paleomagnetic reference frame (Torsvik et al., 2012) (see paleolatitude.org, Van Hinsbergen et al., 2015). The sediments are devoid of biogenic calcium carbonate, but rich in immature organic matter, including terrestrial and marine

microfossil assemblages and molecular fossils (e.g. Pagani et al., 2006; Sluijs et al., 2006; Stein et al., 2006).

As the upper Paleocene and lower Eocene sediments of the ACEX core lack biogenic calcium carbonate and alkenones, SST reconstructions are based on the biomarker-based paleothermometer TEX_{86}. This proxy is based on membrane lipids (isoprenoid glycerol dibiphytanyl glycerol tetraethers; isoGDGTs) of Thaumarchaeota, which adapt the fluidity of their membrane according to the surrounding temperature by increasing the number of cyclopentane rings at higher temperatures (De Rosa et al., 1980; Wuchter et al., 2004; Schouten et al., 2013, and references therein). The proxy was introduced in 2002 by Schouten et al. (2002) and was calibrated to mean annual SST using modern marine surface sediments.

Initial papers suggested that Arctic SST increased significantly during two episodes of transient global warming. Maximum values of ~23°C and ~27 °C occurred during the Paleocene-Eocene Thermal Maximum (PETM-56 Ma ago, Sluijs et al., 2006) and Eocene Thermal Maximum 2 (ETM2-54 Ma ago, Sluijs et al., 2009), respectively. Lower SSTs, generally exceeding 20 °C, characterized the remainder of the early Eocene (Sluijs et al., 2008b). Such temperatures were immediately recognized to be remarkably high and could not be explained using fully-coupled climate model simulations (Sluijs et al., 2006). Even the current-generation of IPCC-class models are unable to match early Eocene Arctic mean annual SSTs, although reconstructions of tropical and mid-latitude SSTs and deep ocean temperatures are consistent with some newer simulations (Frieling et al., 2017; Cramwinckel et al., 2018; Evans et al., 2018; Zhu et al., 2019).

Since the publication of the ACEX SST records, constraints on the applicability of the TEX_{86} proxy have tremendously improved (see review by Schouten et al., 2013, and

subsequent work by Taylor, 2013 #1645; Elling et al., 2014; Qin et al., 2014; Elling et al., 2015; Kim et al., 2015; Qin et al., 2015; Hurley et al., 2016; Zhang et al., 2016). This work has delivered new constraints on the ecology of Thaumarchaeota, the dominant depth at which they reside in the ocean and from which depth their isoGDGTs are exported towards the sea floor. It also identified potential confounding factors such as variation in dominant isoGDGT export depth (e.g., Taylor et al., 2013; Kim et al., 2015), the input of non-Thaumarchaeotal-derived isoGDGTs (e.g., Weijers et al., 2011; Zhang et al., 2011), growth phase (Elling et al., 2014), and environmental ammonium and oxygen concentrations (Qin et al., 2015; Hurley et al., 2016). Moreover, several indicators to detect such anomalies have been developed. Improvements in the chromatography method used for GDGT analysis now allow for better separation of previously co-eluting compounds leading to enhanced analytical precision and sensitivity (Hopmans et al., 2016). Finally, recent work has described new GDGTs from oceans and sediments, notably branched glycerol monoalkyl glycerol tetraethers (brGMGTs, or 'H-shaped' brGDGTs) (e.g., Schouten et al., 2008; Liu et al., 2012), characterized by a covalent carbon-carbon bond that links the two alkyl chains. Their presence and distribution in peats and lake sediments has been linked to land air temperatures (LAT) (e.g., Naafs et al., 2018a; Baxter et al., 2019). However, these compounds have not yet been reported from ancient marine sediments.

Considering these developments and the paleoclimatological importance of the ACEX dataset, we re-analyzed the original lipid extracts for the PETM, ETM2 and the interval spanning these events (Sluijs et al., 2006; Sluijs et al., 2009), according to the latest chromatography protocols. We also compile published and generate new GDGT data from modern and Paleogene terrestrial deposits and use these to better assess the

potential confounding influence of isoGDGTs from terrestrial sources, which was already recognized as a potential problem in the early work (Sluijs et al., 2006).

2. GDGT-based SST indices, calibration and confounding factors

2.1 TEX_{86} and its calibration to SST

TEX_{86} is based on the relative abundance of 4 different GDGTs (Figure 2), following (Schouten et al., 2002):

$$TEX_{86} = \frac{([GDGT-2]+[GDGT-3]+[Crenarchaeol\ isomer])}{([GDGT-1]+[GDGT-2]+[GDGT-3]+[Crenarchaeol\ isomer])} \quad \text{Eq. (1)}$$

where a higher relative abundance of cyclopentane moieties implies higher SSTs.

A number of models are used to calibrate TEX_{86} to SST (Schouten et al., 2002; Schouten et al., 2003; Schouten et al., 2007; Kim et al., 2008; Liu et al., 2009; Kim et al., 2010; Tierney and Tingley, 2014; O'Brien et al., 2017), all based on a modern ocean surface sediment database. The currently available culture and mesocosm experiments and surface sediment data suggest that the relation between SST and TEX_{86} is close to linear for a large portion of the modern ocean (Kim et al., 2010; Ho et al., 2014; Tierney and Tingley, 2014; O'Brien et al., 2017). In polar regions, the TEX_{86} response to temperature diminishes (e.g., Kim et al., 2010; Tierney and Tingley, 2014). The response of TEX_{86} to SST at the high temperature end remains subject of discussion (e.g. Cramwinckel et al., 2018; Hollis et al., 2019). Several authors prefer a linear relation (e.g., Tierney and Tingley, 2014; O'Brien et al., 2017). However, physiological considerations and multiple temperature-dependent GDGT indices might imply a non-linear relation also at the high temperature end, as can be observed at the high end of the modern ocean dataset and beyond the reach of the modern ocean in paleoclimate data (Cramwinckel et al., 2018). At higher temperatures, membrane adaptation may

144 increasingly be established using isoGDGTs not included in the TEX_{86} ratio leading to
145 a diminished TEX_{86} response at very high temperatures (Cramwinckel et al., 2018). A
146 non-linear response has thus been proposed in other calibrations (Liu et al., 2009; Kim
147 et al., 2010). The most recent non-linear calibration, TEX_{86}^{H} (Kim et al., 2010),
148 represents an exponential relation between SST and TEX_{86} (Hollis et al., 2019).
149 Unfortunately, TEX_{86}^{H} is mathematically problematic and has systematic residuals in
150 the modern ocean (Tierney and Tingley, 2014).
151 Tierney and Tingley (2014) introduced a spatially-varying Bayesian method to convert
152 TEX_{86} to SST and assumes a linear relationship (BAYSPAR). BAYSPAR extracts
153 TEX_{86} values from the modern core-top dataset that are similar to the measured TEX_{86}
154 value from the geological sample based on a tolerance defined by the user, and
155 subsequently calculates regressions based on these core-top data. The uncertainty in
156 SST reflects spatial differences in the correlation coefficient and intercept and the error
157 variance of the regression model.
158 Currently, it is generally encouraged to present results both using a linear and a non-
159 linear function (Hollis et al., 2019). The assumption of a linear or non-linear relation
160 between SST and TEX_{86} leads to very different SST reconstructions for geological
161 samples yielding TEX_{86} values >0.70 (Kim et al., 2010; Tierney and Tingley, 2014;
162 Frieling et al., 2017; O'Brien et al., 2017; Cramwinckel et al., 2018; Hollis et al., 2019).
163 However, TEX_{86} values of the early Eocene ACEX samples (0.5 – 0.7, Sluijs et al.,
164 2006; Sluijs et al., 2008b; Sluijs et al., 2009) are below this value and well above most
165 values observed in the polar regions (Kim et al., 2010; Tierney and Tingley, 2014;
166 O'Brien et al., 2017), indicating that all calibrations will yield similar absolute SST
167 values.
168

169 *2.2 Caveats and confounding factors*

170 Several confounding factors and caveats have been identified that could potentially bias
171 TEX_{86} data relative to mean annual SST. These notably relate to additions of isoGDGTs
172 that were not produced in the upper water column by Thaumarchaeota, seasonal biases,
173 and choices that are made in the calibration between SST and TEX_{86}. Below we
174 summarize methods that have been developed to assess if isoGDGT distributions might
175 have been biased by confounding factors.

176

177 *2.2.1 isoGDGTs of terrestrial origin*

178 Previous work (Sluijs et al., 2006; Sluijs et al., 2008b; Sluijs et al., 2009) recognized
179 that high contributions of terrestrially-derived isoGDGTs could compromise the TEX_{86}
180 signal for portions of the upper Paleocene to lower Eocene interval of the ACEX core.
181 This contribution can be tracked using the Branched and Isoprenoid Tetraether (BIT)
182 index, a ratio of mostly soil-derived branched GDGTs (brGDGTs; Figure 2) and
183 Crenarchaeol, which is dominantly marine-derived (Hopmans et al., 2004; Schouten et
184 al., 2013):

185 $$BIT\ index = \frac{([brGDGT-Ia]+[brGDGT-IIa]+[brGDGT-IIIa])}{([brGDGT-Ia]+[brGDGT-IIa]+[brGDGT-IIIa])+[Crenarchaeol])} \quad \text{Eq. (2)}$$

186 Most studies define a BIT value (typically 0.3 or 0.4) above which TEX_{86}-derived SST
187 are unreliable (e.g., Weijers et al., 2006). However, the threshold of 0.4 is conservative
188 in some settings and the impact of terrigenous GDGTs on reconstructed SST will
189 depend on the nature and temperature of the source catchment (Inglis et al., 2015). In
190 addition, a cut-off value based on BIT values is difficult given the relatively large
191 differences in BIT between labs, which originate from methodological differences
192 (Schouten et al., 2009). A strong linear relationship between BIT and TEX_{86} values is
193 often taken as indication of a bias in TEX_{86} through land-derived isoGDGTs to the

194 marine TEX_{86} signature (e.g., Douglas et al., 2014). An earlier study used a somewhat
195 subjective threshold of 0.3 for an interval spanning ETM2 in the ACEX core (Sluijs et
196 al., 2009).
197
198 *2.2.2 isoGDGTs of deep water origin*
199 Thaumarchaeota, the source of most isoGDGTs in marine waters (Zeng et al., 2019;
200 Besseling et al., 2020), are ammonium oxidizers (Könneke et al., 2005; Wuchter et al.,
201 2006a), making them independent of light. Although they occur throughout the water
202 column, maximum abundances occur at depths <200 m, generally around NO_2 maxima
203 (e.g., Karner et al., 2001; Pitcher et al., 2011a). In most oceans, sedimentary GDGTs
204 dominantly derive from the upper few hundred meters, based on analyses of suspended
205 particular organic matter and sediment traps (Wuchter et al., 2005; Wuchter et al.,
206 2006b; Yamamoto et al., 2012; Richey and Tierney, 2016). A deeper contribution has
207 also been inferred based on ^{14}C analysis (Shah et al., 2008), implying possible
208 contributions of isoGDGTs from thermocline. Moreover, contributions of isoGDGTs
209 produced in the deep sea have regionally been identified (e.g., Kim et al., 2015). Taylor
210 et al. (2013) also found that deep dwelling (>1000 meter) archaea might contribute to
211 the sedimentary isoGDGT assemblage. They indicate that such deep contributions can
212 be tracked using the GDGT-2/GDGT-3 ratio; high values of >5 indicate contributions
213 of archaea living deeper in the water column. Given that upper Paleocene and lower
214 Eocene ACEX sediments were deposited in a shallow shelf environment (Sluijs et al.,
215 2008b), a significant contribution of deep ocean archaeal lipids is not expected.
216

2.2.3 isoGDGTs of methanotrophic and methanogenic archaea

Contributions of isoGDGTs to the sedimentary pool might also derive from anaerobic methanotrophs and/or methanogens. Several indices have been developed to track such contributions, both based on relatively high contributions of particular isoGDGTs of these groups of archaea. The Methane Index (MI) was developed to detect the relative contribution of anaerobic methanotrophic Euryarchaeota, notably represented by GDGT-1, 2 and 3 (Pancost et al., 2001; Zhang et al., 2011) and is therefore defined as

$$MI = \frac{[GDGT-1]+[GDGT-2]+[GDGT-3]}{([GDGT-1]+[GDGT-2]+[GDGT-3]+[Crenarchaeol]+[Crenarchaeol\ isomer])} \quad \text{Eq. (3)}$$

MI values greater than 0.5 indicate significant contribution of anaerobic methanotrophy. Such values may yield unreliable TEX_{86} values. Another tracer for contributions of anaerobic methanotrophic archaea is the analogous GDGT-2/Crenarchaeol ratio (Weijers et al., 2011).

Methanogenic archaea can synthesize GDGT-0, as well as smaller quantities of GDGT-1, GDGT-2 and GDGT-3. The ratio GDGT-0/Crenarchaeol is indicative of contributions of methanogenic archaea to the isoGDGT pool (Blaga et al., 2009) where values > 2 indicate substantial contribution of methanogenic archaea. Up to now, high index values have often been observed near methane seeps or anoxic basins (e.g., Jaeschke et al., 2012) but rarely in open marine waters in the modern and paleodomains (Inglis et al., 2015; Zhang et al., 2016). Given the reducing conditions in the sediment and water column at the study site across the late Paleocene and early Eocene (Sluijs et al., 2006; Stein et al., 2006; Sluijs et al., 2008b; März et al., 2010), an influence of methane cycling might be expected.

240 *2.2.4 isoGDGTs of the 'Red Sea Type'*

241 Sedimentary isoGDGT distributions from the Red Sea are anomalous to other marine
242 settings and are characterised by the low abundance of GDGT-0 and the high abundance
243 of the Crenarchaeol isomer. Presumably, this is due to an endemic Thaumarchaeotal
244 assemblage. The Red Sea isoGDGT distribution yields a different relationship between
245 SST and TEX_{86} (Trommer et al., 2009; Kim et al., 2015). Inglis et al. (2015) attempted
246 to quantify a 'Red Sea-type' GDGT distribution in geological samples using the
247 following index:

248 $$\%\mathrm{GDGTrs} = \frac{[Crenarchaeol\ isomer]}{([GDGT{-}0] + [Crenarchaeol\ isomer])}\ x\ 100 \qquad \text{Eq. (4)}$$

249 However, as noted by Inglis et al. (2015) this ratio is also strongly SST-dependent such
250 that the Red Sea type GDGT assemblage cannot be discerned from GDGT distributions
251 that occur at high temperatures in normal open marine settings.

252

253 *2.2.5 Seasonal bias*

254 TEX_{86} is calibrated to mean annual SST. However, particularly in mid and high latitude
255 areas where production and export production is highly seasonal, the sedimentary
256 GDGT distribution might not represent annual mean conditions (Wuchter et al., 2006b;
257 Pitcher et al., 2011b; Mollenhauer et al., 2015; Richey and Tierney, 2016; Park et al.,
258 2019). This issue should partly be reflected in the calibration uncertainty of the modern
259 ocean database (several °C, depending on the calibration and method; see section 2.7).
260 Sluijs et al. (2006; 2008b; 2009) originally argued that the TEX_{86} results from the
261 ACEX core could be biased towards summer temperature because the export of organic
262 matter from the surface ocean towards the sediment likely peaked during the season of
263 highest production, i.e., the summer. However, we also note that the TEX_{86}-temperature
264 relationship is not improved when using seasonal mean ocean temperatures (Kim et al.,

2010; Tierney and Tingley, 2014) and modern observations indicate homogenization of the seasonal cycle at depth (Wuchter et al., 2006b; Yamamoto et al., 2012; Richey and Tierney, 2016), implying that seasonality has relatively limited effect on modern sedimentary TEX_{86} values.

2.2.6 Additional isoGDGT-based temperature indicators

The underlying mechanism of TEX_{86} is that isoGDGTs produced at higher SSTs contain more rings than those produced at low SSTs. Although the combination of compounds included in TEX_{86} seems to yield the strongest relation with temperature in the modern ocean (Kim et al., 2010), it implies that isoGDGT ratios other than TEX_{86} also provide insights into SST. One alternative temperature sensitive isoGDGT index is the Ring Index (RI), which represents the weighed number of cyclopentane rings of isoGDGTs 0-3, Crenarchaeol and the Crenarchaeol isomer (Zhang et al., 2016), defined as:

$$RI = 0x[\%GDGT-0] + 1\,x[\%GDGT-1] + 2\,x[\%GDGT-2] + 3\,x[\%GDGT-3] + 4\,x\,[\%Crenarchaeol + \%Crenarchaeol\ isomer] \quad \text{Eq. (5)}$$

Note that the abundance of GDGT-0 is important for determining the percentage of the other GDGTs of the total isoGDGT pool.

The close relation between TEX_{86} and RI can also be used to detect aberrant distributions, including those produced by methanogenic, methanotrophic and terrestrial sources, as these sources typically contribute disproportionate amounts of specific lipids. A RI_{TEX}, calculated from TEX using the polynomial fit of Zhang et al. (2016), is subtracted from the RI to arrive at the ΔRI. Cut-off values for sample deviation from the modern ocean calibration dataset are defined as 95% confidence limits of the TEX_{86}-RI relation, or above |0.3| ΔRI units.

290 *2.3 H-shaped branched GDGTs; brGMGTs*

291 BrGMGTs (Figure 2) were first identified by Liu et al. (2012) in marine sediments, who
292 identified a single acyclic tetramethylated brGMGT (*m/z* 1020). This compound was
293 later detected within the marine water column and appeared to be abundant within the
294 oxygen minimum zone (Xie et al., 2014). Naafs et al. (2018a) identified a larger suite
295 of brGMGTs (including *m/z* 1048 and 1034), in a quasi-global compilation of modern
296 peat samples. They argued that these compounds were preferentially produced at depth,
297 within the anoxic catotelm. Analogous to the continental paleothermometer based on
298 bacterial brGDGTs produced in surface soils, termed MBT'$_{5me}$ (Weijers et al., 2007b;
299 De Jonge et al., 2014), they showed that the degree of methylation of brGMGTs in peats
300 relates to mean annual air temperature. They calculated the degree of methylation of
301 brGDGTs without cyclopentane moieties, designed for comparison to the methylation
302 of brGMGTs, defined by H-MBT$_{acyclic}$:

303

304 $$MBTacyclic = \frac{brGDGT-Ia}{(brGDGT-Ia+brGDGT-IIa+brGDGT-IIa'+brGDGT-IIIa+brGDGT-IIIa')}$$ Eq. (6)

305

306 $$H-MBTacyclic = \frac{brGMGT-H1020}{(brGMGT-H1020+brGMGT-H1034+brGMGT-H1048)}$$ Eq. (7)

307

308 Based on the strong relation between MBT$_{acyclic}$ and H-MBT$_{acyclic}$ in their peat samples,
309 Naafs et al. (2018a) suggested that the brGMGTs have the same origin as the brGDGTs,
310 presumably Acidobacteria (Sinninghe Damsté et al., 2011; Sinninghe Damsté et al.,
311 2018a). In addition, they showed that the abundance of brGMGTs (relative to the total
312 amount of brGMGTs and brGDGTs) positively correlates with mean annual air
313 temperature, suggesting that the covalent bond in the brGMGTs is used to maintain
314 membrane stability at higher temperature (Naafs et al., 2018a).

Baxter et al. (2019) identified a total of seven different brGMGTs from a suite of African lake sediments (Figure 2), and found their relative distribution to correlate to mean annual air temperature. Accordingly, they proposed a proxy for mean annual air temperature termed brGMGT-I (see Figure 2 for the molecular structures referred to here):

$$brGMGT - I = \frac{[H1020c]+[H1034a]+[H1034c]}{[H1020b]+[H1020c]+[H1034a]+[H1034c]+[H1048]} \quad \text{Eq. (8)}$$

3. Material and Methods

We used the polar fractions previously analyzed by Sluijs et al. (2006; 2009) from the PETM through ETM2 interval at IODP Expedition 302 Hole 4A. These fractions originate from a total lipid extract produced using a Dionex Accelerated Solvent Extractor and fraction separations by Al_2O_3 column chromatography using hexane:dichloromethane (DCM) (9:1, *v/v*) and DCM:methanol (1:1; *v/v*) to yield the apolar and polar fractions, respectively. Polar fractions were re-dissolved in hexane:isopropanol (99:1, *v/v*) and passed through a 0.45-µm polytetrafluoroethylene filter. This fraction was then analyzed by high-performance liquid chromatography (HPLC) and atmospheric pressure chemical ionization–mass spectrometry using an Agilent 1260 Infinity series HPLC system coupled to an Agilent 6130 single-quadrupole mass spectrometer at Utrecht University following Hopmans et al. (2016) to measure the abundance of GDGTs. Based on long-term observation of the in-house standard, the analytical precision for TEX_{86} calculates to ±0.3 °C in the SST domain.

To gain further insights into the potential impact of terrestrial isoGDGT input on TEX_{86} values, we compiled isoGDGT and brGDGTs distributions from modern peats (n = 473, Naafs et al., 2017) and early Paleogene lignites (n = 58, Naafs et al., 2018b). Note, the fractional abundance of Crenarchaeol isomer was not reported in the early Paleogene

dataset of Naafs et al. (2018b). We therefore revisited the original chromatograms from Naafs et al. (2018b) and integrated the crenarchaeol isomer (*m/z* 1292).

4. Results

The new GDGT distributions (Supplementary Table) are consistent with the TEX_{86} and BIT index data generated over a decade ago using the older analytical HPLC setup (Hopmans et al., 2000; Hopmans et al., 2016) (Figure 3). TEX_{86} exhibits some scatter and the slope of the regression is slightly off the 1:1 line indicating that the new data have somewhat higher TEX_{86} values. Less scatter is apparent in the BIT record but the original BIT index values were slightly higher than recorded here, as indicated by the regression (Figure 3). This result is consistent with previous analyses with the new analytical setup (Hopmans et al., 2016). This does not impact previous qualitative interpretations of this record (Sluijs et al., 2006; Sluijs et al., 2008b; Sluijs et al., 2009). In the discussion section, we assess indicators of potential confounding factors (section 2.2), including the influx of terrestrially-derived isoGDGTs to the sediments (Figures 4, 5 and S1) and several indices related to methane and depth of production (Figures 6). Although we did not detect significant amounts of isoprenoid GMGTs, high abundances of various brGMGTs are present in the ACEX samples, in total between 10 and 45% of the total brGDGT assemblage (Figure 7). We consistently identify at least five brGMGTs across the three different mass-to-charge ratios (*m/z* 1020, 1034 and 1048). Based on their (relative) retention times and overall distribution we were able to apply the nomenclature of Baxter et al. (2019) to five of these and assign individual peaks to previously identified compounds (Figure S2). The abundance of brGMGTs relative to brGDGTs increase during the PETM. The proposed temperature indicators

364 based on brGMGTs show mixed results, with some showing a clear response to the
365 PETM (Figure 7e) while others do not (Figure 7d).
366
367 **5. Discussion**
368 *5.1 IsoGDGT provenance*
369 *5.1.1 Contributions of soil-derived isoGDGTs*
370 As noted by Sluijs et al. (2006), late Paleocene samples yield anomalously high
371 abundances of GDGT-3, likely derived from a terrestrial source. We therefore consider
372 the late Paleocene temperature estimates unreliable. To assess the temperature change
373 during the PETM, Sluijs et al. (2006) developed a TEX_{86} calibration without this
374 moiety, termed TEX'_{86}. However, TEX'_{86} has not been widely used outside the
375 Paleogene Arctic because the anomalous abundances of GDGT-3 have not been
376 recorded elsewhere. High contributions of GDGT-3 from terrestrial input would also
377 be associated with an increase in the abundance of other isoGDGTs. Indeed, recent
378 TEX_{86}-based global SST compilations and comparison to climate simulations for the
379 PETM excluded the Paleocene ACEX data because the TEX_{86}' calibration complicates
380 the comparison to other regions where it has not been applied (Frieling et al., 2017;
381 Hollis et al., 2019).
382 Input of soil organic matter is consistent with Willard et al. (2019) who established that
383 the brGDGT assemblage is dominantly soil-derived as opposed to being produced in
384 the coastal marine environment. This observation is based upon the weighted average
385 number of rings in the tetramethylated brGDGTs ($\#rings_{tetra}$) which generally does not
386 exceed 0.4 to 0.7 in the global soil calibration dataset (Sinninghe Damsté, 2016). In the
387 ACEX record, $\#rings_{tetra}$ is < 0.21 (Willard et al., 2019), consistent with a dominant soil
388 source. This indicates that 1) brGDGT abundances, 2) brGDGT distributions and 3) the

389 BIT index are reliable indicators of the relative supply of terrestrially-derived
390 isoGDGTs into the marine basin. The Paleocene section of the dataset also stands out
391 regarding its relation between BIT index and TEX_{86} (Figure 4), which confirms its
392 anomalous nature.
393 During the PETM, TEX_{86} values are higher (due to warming) and BIT values lower.
394 This was attributed to sea level rise during the hyperthermals resulting in a more distal
395 position relative to the terrestrial GDGT source (Sluijs et al., 2006; Sluijs et al., 2008a).
396 The interval between 371.0 and 369.0 mcd (i.e. above the PETM and below ETM2)
397 also stands out. This interval was previously recognized by Sluijs et al. (2009) to reflect
398 an open marine environment, with a dominance of marine palynomorphs and algal
399 biomarkers. They also found that high BIT values correspond to low TEX_{86} values
400 within that interval and therefore implemented a subjective threshold value of 0.3,
401 above which TEX_{86}-derived SSTs were considered unreliable. Although the relation
402 between BIT and TEX_{86} exhibits considerable much scatter, the new analyses supports
403 the notion that higher influx of terrestrial isoGDGTs lowers TEX_{86} values. The linear
404 regression (Figure 4; excluding the one outlier with high TEX_{86} and BIT values in the
405 top right of the plot because it has highly anomalous distributions ($\Delta RI = 0.61$)), yields
406 an R^2 of 0.26 so explains a portion of the variation (Figure 4). The nature of this
407 influence is determined by the relative abundance of terrestrial isoGDGTs and their
408 TEX_{86} value. The TEX_{86} value at the terrestrial endmember of BIT = 1, assuming
409 various types of regressions, centers around 0.5. The remainder of the data does not
410 show a clear relation between BIT and TEX_{86} although some of the lowest TEX_{86}
411 values correspond to high BIT values, suggesting that the terrestrial endmember
412 contributed isoGDGT assemblages with relatively low TEX_{86} values in other intervals
413 as well.

414 The relatively low degree of cyclization in the early Eocene contrasts starkly with high
415 degree of cyclisation during the late Paleocene (Figure 6e). This implies that the
416 distribution of terrestrial isoGDGTs varies strongly between the latest Paleocene and
417 early Eocene within our studied section.
418 The impact of soil-derived isoGDGTs also emerges from the Ring Index approach of
419 Zhang et al. (2016, see section 2.2.6 and Figure 6). The difference between the Ring
420 Index and TEX_{86} at the onset of the PETM is mainly controlled by Crenarchaeol, which
421 is comparatively low in abundance in the Paleocene but highly abundant in the PETM.
422 This increase is likely associated with sea level rise during the PETM because
423 Crenarchaeol is predominantly produced in the marine realm. It is also consistent with
424 a drop in BIT index values and the relative abundance of terrestrial palynomorphs
425 (Sluijs et al., 2008a). The approach of Zhang et al. (2016) also confirms that many
426 isoGDGT distributions exhibit an anomalous relation between TEX_{86} and the Ring
427 Index relative to the modern core top dataset, with ΔRI values >0.3 (Figure 6).
428 Importantly, all samples with ΔRI values >0.3 have BIT values above 0.35, indicating
429 that contributions of soil-derived iso-GDGTs dominate non-temperature effects in the
430 distributions. We therefore discard TEX_{86}-derived SSTs for samples with BIT values
431 >0.35.
432 We also develop a crude model to further constrain the potential contribution of
433 terrestrially-derived isoGDGTs. First, we determine the abundance of isoGDGTs
434 relative to brGDGTs in modern peat samples (Naafs et al., 2017) and early Paleogene
435 lignites (fossil peat) (Naafs et al., 2018b, the isoGDGT data are published here).
436 Although there is no reason to assume that peat was a major component of the
437 hinterland (Willard et al., 2019) , the aforementioned datasets can provide an estimate
438 of the potential contribution from terrestrial isoGDGTs to our study site. The raw signal

intensity of brGDGTs in the ACEX samples are used to estimate the potential contribution of terrestrially-derived isoGDGTs to the samples. To this end, we use the fractional abundance of the various isoGDGTs in the modern peat and Paleogene lignite datasets (Figure 5). Then, we estimate the abundance of these terrestrially-derived isoGDGTs in our ACEX samples by scaling this fraction to the measured abundances of brGDGTs and isoGDGTs in our ACEX samples, following

$$Terrestrial\ fraction\ of\ isoGDGT\ \mathrm{x} = \left(Fraction\ of\ isoGDGT\mathrm{x}\ in\ terrestrial\ test\ dataset * \frac{sum(brGDGTs))}{abundance\ of\ isoGDGT\ x}\right) \quad \text{Eq. (9)}$$

where x represents the specific analyzed GDGT (see Supplementary Data File for an example of these calculations).

This leads to estimates of the potential relative contributions of the individual isoGDGTs derived from land in the ACEX samples based on the entire modern peat dataset (Naafs et al., 2017), modern peats from regions with MAT exceeding 15°C (Naafs et al., 2017) and Paleogene lignites (Naafs et al., 2018b, this paper, Figures 5 and S1). This approach implies that Crenarchaeol and the Crenarchaeol-isomer are almost exclusively from the marine realm. However, GDGT-1, GDGT-2 and GDGT-3 in our study site may be derived from the terrestrial realm (Figure 5), especially in specific stratigraphic intervals (Figure S1). In the most extreme cases, the modeled contributions of terrestrial isoGDGTs is higher than the measured isoGDGT abundances (i.e., terrestrial fraction > 1). This is principally seen in isoGDGT-2 and GDGT-3, especially when we employ the Paleogene lignite database. This particular assumption clearly overestimates the abundance of terrestrially sourced isoGDGTs in our setting. However, the temporal trends obtained using modern peats, subtropical modern peats and Paleogene lignites are essentially identical and give some indication which isoGDGTs are most likely to be impacted by terrestrial input and across which

464 intervals. Interestingly, this approach also suggests that particularly GDGT-3 is shown
465 to be strongly affected (Figure 5), which qualitatively matches the distributions in the
466 ACEX samples. This is principally because GDGT-3 is the least abundant marine
467 isoGDGT included in our analyses, whereas it is often as abundant as GDGT-1 and 2
468 in terrestrial settings (Fig. 5).
469
470 *5.1.2 Contributions of methanotrophic or methanogenic archaea?*
471 The depositional environment at the study site included ample (export) production,
472 sediment organic matter content, and low oxygen conditions at the sediment-water
473 interface (Sluijs et al., 2006; Stein et al., 2006; Stein, 2007; Sluijs et al., 2008b; Sluijs
474 et al., 2009; März et al., 2010). This may have been suitable for abundant methanogenic
475 and methanotrophic archaea, potentially contributing to the sedimentary isoGDGT
476 assemblage. However, our GDGT-2/Crenarchaeol values (<0.23; Figure 6) are far
477 below values that suggest significant isoGDGT contributions of methanotrophic
478 Euryarchaeota as described by Weijers et al. (2011). MI values (maximum observed
479 0.31) are also generally below proposed cut off values (0.3-0.5, Zhang et al., 2011) that
480 suggest such contributions. Finally, GDGT-0/Crenarchaeol ratios (<1.4) remain below
481 the cut-off value of 2 throughout the section (Figure 6), also making a significant
482 isoGDGT contribution from methanogens highly unlikely (Blaga et al., 2009).
483 Collectively, relative contributions of isoGDGTs from methanogenic and
484 methanotrophic archaea seem low despite the low-oxygen environment, suggesting a
485 relatively high flux of pelagic isoGDGTs.
486
487 *5.1.3 Contributions of deep-dwelling archaea?*

Taylor et al. (2013) showed that GDGT-2/GDGT-3 ratios correspond to depth of production, with high values (>5) in deep waters (>1000 m). We record low values (1-4) between ~390 and ~371.2 mcd (Figure 6), which supports a dominant production in the surface ocean based on the modern calibration data set (Taylor et al., 2013). However, the overlying interval (~371 to ~368.3 mcd) has much higher (average 7.4) and variable GDGT-2/GDGT-3 values with peak values of 10-14. Such values suggest significant contributions of isoGDGTs produced at water depths of several kilometers according to the analyses by Taylor et al. (2013).

However, all paleoenvironmental information generated based on the sediments as well as tectonic reconstructions of Lomonosov Ridge – a strip of continental crust that disconnected from the Siberian margin in the Paleocene - has indicated a neritic setting of the drill site at least up to the middle Eocene (e.g., O'Regan et al., 2008; Sangiorgi et al., 2008; Sluijs et al., 2008a; Sluijs et al., 2009). At ~371.2 mcd a drop in BIT index and a change in the palynological assemblages corresponds to an interval of greenish sediment, suggestive of pronounced amounts of glauconite. These changes are consistent with local relative sea level rise, causing a somewhat more distal position relative to the shoreline. However, the sediment remains dominantly siliciclastic and organic terrestrial components, particularly pollen and spores, remain abundant still indicating a shallow setting (Sluijs et al., 2008a; Sluijs et al., 2008b). Increased contributions of isoGDGTs produced at depth would be expected to have caused a systematic cold bias but based on linear regression analysis the large variability in GDGT-2/GDGT-3 ratios is unrelated to the recorded variability in TEX_{86} values. The high GDGT-2/GDGT-3 ratio values can therefore not be explained by contributions of deep dwelling archaea.

In a study of the last 160 kyr in the South China Sea, Dong et al. (2019) found that very high GDGT-2/GDGT-3 ratios (~9 but up to 13) correspond with high values in nitrogen isotope ratios, interpreted to reflect low contributions in diazotroph N_2 fixation and enhanced upwelling. In our record, the high GDGT-2/GDGT-3 ratios are associated with normal marine conditions and the dinocyst assemblages are not indicative of upwelling conditions (Sluijs et al., 2009). Unfortunately, the available nitrogen isotope record (Knies et al., 2008) does not cover this interval in sufficient resolution to assess a relation with diazotroph activity. The increase in GDGT-2/GDGT-3 ratio correlates to a strong drop in BIT index values and an increase in normal marine dinocyst species (Sluijs et al., 2009), but a shift to more open marine environment does not explain the high ratio values. As such, the cause of the high GDGT-2/GDGT-3 ratios in this interval remains unclear but we consider it highly unlikely to relate to contributions of deep dwelling Thaumarchaeota.

5.1.4 Oxygen concentrations and ammonium oxidation rates

A variety of non-thermal factors can impact TEX_{86} values, including ammonium and oxygen concentrations and growth phase (Elling et al., 2014; Qin et al., 2014; Hurley et al., 2016). Across the studied interval of the ACEX core, several intervals of seafloor and water column anoxia have been identified based on organic and inorganic proxies, notably during the PETM and ETM2 (Sluijs et al., 2006; Stein et al., 2006; Sluijs et al., 2008b; Sluijs et al., 2009; März et al., 2010).

Particularly suspect is an interval of low TEX_{86} values that marks the middle of the ETM2 interval, directly following a ~4 °C warming at its onset (Sluijs et al., 2009). This interval is also marked by the presence of sulfur-bound isorenieratane (Sluijs et al., 2009), a derivative of isorenieratene. This biomarker is produced by the brown

strain of green sulfur bacteria that require light for photosynthesis and free sulfide, indicating euxinic conditions in the (lower) photic zone (Sinninghe Damsté et al., 1993). We also record a concomitant shift in several methane-related indicators, GDGT-2/GDGT-3 ratio values and the ΔRI. A mid-ETM2 cooling signal has not been recorded at other study sites and this interval marks the occurrence of pollen of thermophilic plants such as palms and baobab (Sluijs et al., 2009; Willard et al., 2019). Therefore, the low TEX_{86} values were suggested to reflect thaumarcheotal depth migration to the deeper chemocline due to euxinic conditions (Sluijs et al., 2009), similar to the modern Black Sea (Coolen et al., 2007; Wakeham et al., 2007) and the Mediterranean Sea during sapropel formation (Menzel et al., 2006).

More recent work has indicated that the isolated marine Thaumarchaeotal species *Nitrosopumilus maritimus* produces lower TEX_{86} values with higher ammonia oxidation rates (Hurley et al., 2016) and O_2 concentrations (Qin et al., 2015). Although this observation is difficult to extrapolate to the total response of the Thaumarcheotal community in the marine environment on geological time scales, lower O_2 availability should lower oxidation rates leading to higher TEX_{86} values (Qin et al., 2015; Hurley et al., 2016). However, we record a drop in TEX_{86} values with the development of anoxia during ETM2. The nature of the anomalously low cyclization in the ETM2 isoGDGT assemblage, which passes all quality tests regarding GDGT distribution (Figure 6), remains therefore elusive.

5.2 Origin and environmental forcing of brGMGTs

The relative abundances of brGMGTs in our samples are surprisingly high. On average, they comprise 25% of the total branched GDGT and GMGT assemblage. The limited literature on modern occurrences implies that both terrestrial and marine sources may

have contributed to the brGMGT assemblage. Data from marine sediments (Liu et al., 2012) and the water column (Xie et al., 2014), clearly shows production within the marine realm. Their occurrence in modern peats (Naafs et al., 2018a), lake sediments (Baxter et al., 2019) and Paleogene lignites (Inglis et al., 2019) might also imply transport from land to marine sediments. A soil-derived source is currently unsupported, as they were most often below detection limit in recent studies of geothermally heated soils (De Jonge et al., 2019) and a soil transect from the Peruvian Andes (Kirkels et al., 2020). The brGMGT abundances we record are close to the maximum abundance found in modern peats (Naafs et al., 2018a). However, significant input of peat-derived organic matter into our study site is inconsistent with the low input of peat-derived *Sphagnum* spores (Willard et al., 2019). Alternatively, the high abundance of brGMGTs could also be related to subsurface production in marine sediments. An analogous process was invoked by Naafs et al. (2018a) to explain very high abundance of brGMGTs in an early Paleogene lignite. Collectively, however, we surmise that production in the marine realm may be an important contributor to the brGMGT pool in our setting.

Several factors may contribute to the rise in the abundance of brGMGTs relative to brGDGTs across the PETM. Higher relative abundances of brGMGTs in modern peats generally occur at higher mean annual air temperatures (Naafs et al., 2018a) and so this signal could relate to warming during the PETM if their origin at the study site is terrestrial. However, since we consider it likely that a large part of the brGMGTs assemblage is of marine origin, the rise in brGMGT abundance likely relates to the previously recorded (Sluijs et al., 2006; Sluijs et al., 2008b) sea level rise during the PETM at the study site. This is consistent with the increase in marine brGMGT production relative to terrestrial brGDGT supply to the study site (Figure 7b). This is

consistent with the inverse correlation between brGMGT abundance and the BIT index (Figure 7b). Lastly, if the production of marine brGMGTs was focused in oxygen minimum zones (Xie et al., 2014), the development of low oxygen conditions in the water column based on several indicators, such as the presence of isorenieratane (Sluijs et al., 2006), might have increased the production of brGMGTs in the water column. It is also possible that all of these factors contributed to the changes in abundance of brGMGTs relative to brGDGTs across the PETM.

The brGMGT-I proxy does not produce temperature trends similar to those seen in TEX_{86} or MBT'_{5me} (Figure 7d). If the majority of the brGMGTs are of marine origin, this indicates that brGMGTs produced in the marine realm do not respond to temperature as was hypothesized based on the African Lake dataset by Baxter et al. (2019).

Also the application of the $H\text{-}MBT_{acyclic}$ index (equation 7) appeared problematic because, similar to Baxter et al. (2019), we identified several more isomers than Naafs et al. (2018a, who developed this index) detected in their peat samples. It therefore remains unclear which of our peaks should be used to calculate the $H\text{-}MBT_{acyclic}$ index values. We therefore show the two plausible options. For the first, we use all peaks with *m/z* 1020, 1034 and 1048 (*H-MBT-all* in Figure 7e) within the expected retention time window. However, based on our chromatography, we consider it more likely that the dominant peaks identified by Naafs et al. (2018a) at *m/z* 1020 and 1034 represent H1020c and H1034b, respectively, and therefore use only those in addition to the single identifiable peak at *m/z* 1048 as a second option (H-*MBT* (H1020*c*, *H1034b*) in Figure 7e. Both options show a clear rise across the PETM, although the HMBT (H1020c, H1034a) shows a larger signal and somewhat better correspondence in absolute values to $MBT_{acyclic}$, though with more scatter. A close correspondence between MBT*acyclic*

612 and HMBT has also been found in a lignite that has been assigned to the PETM (Inglis
613 et al., 2019).
614 If the dominant source of the brGMGTs was marine throughout the record, the increase
615 in methylation possibly relates to warming. This would not be unprecedented as marine-
616 produced brGDGTs show an increase in methylation as a function of temperature
617 (Dearing Crampton-Flood et al., 2018). Sollic et al. (2017) also suggest that archaeal-
618 derived isoprenoid GMGTs produced in marine sediments incorporate additional
619 methyl groups at higher sediment temperatures. Water column oxygen concentrations
620 and pH also changed at our site during the PETM, which potentially affected
621 distributions. Extensive evaluation of brGMGT distributions in modern samples is
622 therefore required to assess the proxy potential.
623
624 *5.3 Uncertainty on TEX_{86}-based SST estimates.*
625 *5.3.1 Uncertainty based on calibration dataset*
626 To calculate SSTs, we use 1) the BAYSPAR method (Tierney and Tingley, 2014),
627 which assumes a linear relationship between TEX_{86} and SST, and 2) TEX_{86}^{H} (Kim et
628 al., 2010), which assumes a non-linear relationship between TEX_{86} and SST.
629 Differences between these calibrations are smaller than the calibration errors (Figure 6)
630 because the TEX_{86} values in the ACEX dataset all fall within the range of the modern
631 core top calibration. Taken together, both indices imply that mean annual SSTs varied
632 between 18 °C and 28 °C in the early Eocene, providing strong evidence for remarkable
633 early Eocene warmth in the Arctic region.
634 The TEX_{86}^{H} calibration has a calibration error of 2.5 °C (residual mean standard error;
635 RSME) (Kim et al., 2010). The BAYSPAR method yields possible values that range
636 ~6 °C from the most probable value (Figure 6), but these uncertainty estimates are more

637 comparable than is immediately apparent, as this analysis takes a 90% confidence
638 interval compared to the 68% probability of RSME. All of the calibrations and methods
639 to obtain values and uncertainties are based on a modern core-top dataset and thus
640 implicitly include potential confounding factors such as seasonality and depth of
641 production and export. However, there is no (quantitative) constraint on any of these
642 parameters in the calibration data set. This is particularly important for the studied
643 region because it represents a polar endmember of the marine environment with highly
644 seasonal production and export and potentially high seasonality in temperature. In the
645 modern ocean, relations between SST and TEX_{86} in the Arctic and ice-proximal
646 Southern Ocean settings differ from the global ocean. This is attributed to a change in
647 viscoelastic adaptation to temperature at the low end and/or a change in the
648 Thaumarchaeotal community (Kim et al., 2010; Ho et al., 2014; Tierney and Tingley,
649 2014). This may mask potential confounding factors that may be relevant specifically
650 to polar environments. This is important here, where the polar regions were ice free and
651 the functioning of physical, chemical and biological ocean systems were fundamentally
652 different from present day. This uncertainty is not accounted for using traditional
653 regression analyses or Bayesian techniques and quantification of uncertainty in non-
654 analogue climates remains extremely difficult.
655
656 *5.3.2 Constraints from independent proxy data*
657 Independent proxy data may provide additional constraints. The appearance of the
658 dinoflagellate cyst genus *Apectodinium* during the PETM and ETM2 in the Arctic basin
659 (Sluijs et al., 2006; Sluijs et al., 2009; Harding et al., 2011) provide qualitative support
660 for pronounced warming and apparent subtropical conditions. Recent efforts to quantify
661 the paleoecological affinities of this now extinct genus have suggested a required

662 minimum temperature of ~20°C (Frieling et al., 2014; Frieling and Sluijs, 2018).
663 Although this value is partly based on TEX_{86} data from the ACEX cores, it is supported
664 by data from an epicontinental site in Siberia (Frieling et al., 2014).
665 A second line of independent proxy evidence includes vegetation reconstructions. As
666 indicated above, the TEX_{86} results are qualitatively consistent with the ample evidence
667 for thermophilic plants and animals in the Arctic (e.g., Heer, 1869; Schweitzer, 1980;
668 Greenwood and Wing, 1995; Uhl et al., 2007; Suan et al., 2017). Particularly valuable
669 are minimum winter temperature tolerances for specific plant species. Palynological
670 analyses have indicated the presence of palm and baobab pollen within the PETM and
671 ETM2 intervals in the ACEX cores (Sluijs et al., 2009; Willard et al., 2019). Modern
672 palms are unable to tolerate sustained intervals of frost and sexual reproduction is
673 limited to regions where the coldest month mean temperature (CMMT) is significantly
674 above freezing (Van der Burgh, 1984; Greenwood and Wing, 1995). This threshold was
675 was recently quantified to be ≥ 5.2 °C (Reichgelt et al., 2018). The presence of baobab
676 within the PETM interval and ETM2 also indicate mean winter air temperatures of at
677 least 6 °C (Willard et al., 2019). Importantly, these plants were not encountered in the
678 intervals outside the PETM and ETM2, suggesting background coldest month mean air
679 temperatures were potentially too low (<6ºC) to support megathermal vegetation.
680 Pollen of palms and *Avicennia* mangroves were recently identified in time-equivalent
681 sections in Arctic Siberia (Suan et al., 2017). Although the details of stratigraphic
682 framework for these records may be somewhat problematic, these findings indicate
683 elevated CMMT estimates on land (>5.5 °C) and in the surface ocean (>13 °C) during
684 the late Paleocene and early Eocene (Suan et al., 2017).
685 Apparently conflicting evidence comes from the occurrence of glendonites and erratics
686 in specific stratigraphic levels in Paleocene and Eocene strata in Spitsbergen,

687 interpreted to reflect ‘cold snaps’ in climate (Spielhagen and Tripati, 2009). Some of
688 these stratigraphic levels are very close to (or even potentially within) the PETM,
689 considering the local stratigraphic level of the PETM (Cui et al., 2011; Harding et al.,
690 2011). However, glendonites and erratics have not been found at the exact same
691 stratigraphic levels as thermophilic biota (Spielhagen and Tripati, 2009). The formation
692 and stability of ikaite (the precursor mineral of the diagenetic glendonites) in
693 Spitsbergen was dependent on relatively low temperature, arguably persistent near-
694 freezing sea water temperatures in the sediment (Spielhagen and Tripati, 2009).
695 However, glendonite occurrences in other settings (e.g. Mesozoic sediments in mid-
696 latitude regions, Teichert and Luppold, 2013) have recently also been linked to methane
697 seeps (Morales et al., 2017). Therefore, the specific temperature constraints implied by
698 glendonites under such conditions are subject of debate. Future work should apply
699 temperature reconstructions based on the geochemical composition of the glendonites,
700 and biomarkers or biota on corresponding strata to assess whether glendonite
701 occurrence is related to colder climates.
702 The estimate on seasonal minima provides an important constraint on Arctic
703 climatology during the PETM and ETM2. Most likely, the palms and baobabs grew
704 close to the shore, where the relative heat of the ocean kept atmospheric temperatures
705 relatively high during the winter. If minimum winter SSTs were in the range of the SST
706 reconstructions based on the nearby *Avicennia* mangrove pollen (Suan et al., 2017),
707 which for open ocean settings would perhaps amount to ~10 °C, then summer SST must
708 have soared to at least 30 °C in summer if TEX_{86}–based SST reconstructions of ~20 °C
709 truly reflects the annual mean. It would imply an SST seasonality of ~20 °C, much
710 higher than any modern open marine setting. In the present day Arctic Ocean, heat is
711 seasonally stored and released in sea ice melting and freezing, and sea ice cover

712 insulates the ocean and reflects much sunlight, resulting in a seasonal cycle of not more
713 than 1.5 °C, even in ice-free regions (Chepurin and Carton, 2012). However, coupled
714 model simulations have indicated that the future loss of sea ice will greatly enhance the
715 seasonal SST range to up to 10 °C in 2300 given unabated CO_2 emissions (Carton et
716 al., 2015). With year-round snow and ice-free conditions, even stronger summer
717 stratification during the Eocene due to higher greenhouse gas concentrations and fresh-
718 water supply through an enhanced hydrological cycle (Pierrehumbert, 2002;
719 Carmichael et al., 2017), a near-shore 20 °C seasonal cycle in Arctic Ocean SST may
720 not be unrealistic, although it remains inconsistent with current-generation fully
721 coupled, relatively low resolution, model simulations (e.g., Frieling et al., 2017).
722 Constraints from the total pollen assemblages in the ACEX cores based on a nearest
723 living relative approach suggest Arctic mean annual temperatures on land of 13-18 °C,
724 and summer temperatures significantly exceeding 20 °C during the PETM and ETM2
725 (Willard et al., 2019). Although these estimates come with much larger uncertainty than
726 winter temperatures and may suffer from the non-analogous setting, they are generally
727 lower than our TEX_{86} values. The brGDGT-based paleothermometer MBT'_{5me} (De
728 Jonge et al., 2014) also suggests lower mean annual air temperatures than reported from
729 TEX_{86} (Willard et al., 2019, Figure 7). These data, derived from the same UHPLC/MS
730 analyses as the isoGDGT data presented here, indicate mean annual air temperatures
731 averaging ~18 °C during the PETM, with a residual mean calibration error of 4.8 °C.
732 This value is ~7 °C lower than earlier estimates based on a slightly different method,
733 analytical procedure and a smaller modern calibration dataset (Weijers et al., 2007a).
734 However, recent inclusion of data from Indian soils in the MBT'_{5me} calibration dataset
735 improved the proxy at the higher temperature end (Dearing Crampton-Flood et al.
736 2020). The new calibration, BayMBT, results in air temperatures ~3 °C higher than that

737 of De Jonge et al. (2014), which was used by Willard et al. (2019; Figure 7). The high
738 calibration uncertainty of MBT (Supplementary Table) implies that the biomarker-
739 derived air temperature and SST reconstructions are within error.
740
741 *5.4 State of constraints on Paleocene-Eocene Arctic temperatures*
742 To unlock the unique premise of Eocene climates for testing the skill of current-
743 generation fully coupled climate models under high greenhouse gas forcing, proxy data
744 and models are ideally approached separately. Among the most important implications
745 of the Arctic temperature estimates are reconstructions of the meridional temperature
746 gradients. Importantly, not a single simulation using an IPCC-class model of early
747 Paleogene climate has produced Arctic annual mean sea surface temperatures close to
748 the ACEX TEX_{86}-based reconstructions without unrealistically high tropical SSTs
749 (Lunt et al., 2012). Recent simulations using the Community Earth System Model
750 (CESM) versions 1 (Frieling et al., 2017; Cramwinckel et al., 2018) and 1.2 (Zhu et al.,
751 2019) using Eocene boundary conditions produced climates that correspond to SST
752 reconstructions in many ocean regions based on several proxies, but still produced
753 cooler mean annual SSTs for the Arctic Ocean than suggested by TEX_{86} (Frieling et al.,
754 2017; Cramwinckel et al., 2018; Zhu et al., 2019). TEX_{86} also indicates SSTs higher
755 than in these model simulations at several sites along the Antarctic margin (Bijl et al.,
756 2009; Bijl et al., 2013). The question thus remains if the conversion of TEX_{86} values
757 towards mean annual SST using any modern core-top calibration for high latitude
758 Paleogene locations is valid, or if the climate models still significantly underestimate
759 polar temperatures. Certainly, if interpreted as mean annual SST, TEX_{86}-based
760 estimates are high compared to the few available additional estimates, notably based on
761 vegetation, but the latter also suffer from similar uncertainties (e.g., Hollis et al., 2019).

A few biases might lead to underestimates of meridional temperature gradients as indicated from TEX_{86}. First, the flat Eocene temperature gradient implied by TEX_{86} was suggested to result from erroneously calibrating the proxy to SST rather than to the temperature of the subsurface (Ho and Laepple, 2016). The rationale is that the meridional temperature gradient is smaller in deeper waters than it is in the surface. However, the idea was contested for multiple reasons, including the fact that sediments at most Eocene study sites, such as the ACEX site, were deposited at a depth of less than 200m, making the application of a deep subsurface (>1000m) calibration inappropriate (Tierney et al., 2017). Moreover, recent analyses have indicated that the TEX_{86} signal dominantly reflects temperature of top 200 m of the water column (Zhang and Liu, 2018).

Secondly, as suggested previously (Sluijs et al., 2006), if TEX_{86} were biased towards any season in the non-analogue Arctic Ocean, it would be the summer, the dominant season of organic matter export towards the seafloor through fecal pelleting or marine snow aggregates. Vegetation suggests very high winter continental coldest month mean air temperatures of at least 6-8 °C (Sluijs et al., 2009; Suan et al., 2017; Willard et al., 2019), coastal coldest month mean SSTs of >13 °C (Suan et al., 2017), and terrestrial mean annual and warmest month mean temperature on land of 13-21 °C and >20°C, respectively (Suan et al., 2017; Willard et al., 2019) (see section 5.3.2). These estimates are closer to the most recent model simulations and lower than the existing TEX_{86} (e.g., Frieling et al., 2017; Zhu et al., 2019). If TEX_{86}-implied SST of ~25 °C is skewed towards a summer estimate, this would decrease the model-data bias regarding the meridional temperature gradient estimates. Given the current uncertainties in the use of TEX_{86} for the non-analogue Arctic Ocean, we however cannot independently constrain this.

6. Conclusions

We analyzed isoGDGT and brGMGT (H-shaped brGDGT) distributions in sediments recovered from the Paleocene-Eocene Thermal Maximum (PETM; ~56 Ma) to Eocene Thermal Maximum 2 (ETM2; ~54 Ma) interval on Lomonosov Ridge, Arctic Ocean using state-of-the-art analytical procedures, compare them to the original dataset (Sluijs et al., 2006; Sluijs et al., 2009) and interpret the results following the currently available TEX_{86} proxy constraints.

Although contributions of isoGDGTs from land complicate TEX_{86} paleothermometry in some stratigraphic intervals, temperature was the dominant variable controlling TEX_{86} values. Background early Eocene SSTs exceed ~20 °C and peak warmth occurred during the PETM and ETM2. However, uncertainty estimates of these SSTs based on the non-analogue modern ocean, remains complex. Temperature constraints from terrestrial vegetation support remarkable warmth in the study section and elsewhere in the Arctic basin, notably coldest month mean temperatures around 10 °C at least within the PETM and ETM2. If TEX_{86}-derived SSTs of ~20 °C truly represent mean annual SSTs, the seasonal range of Arctic SST might have been in the order of 20 °C. If SST estimates are entirely skewed towards the summer season, seasonal ranges in the order of 10 °C may be considered comparable to those simulated in future ice-free Arctic Ocean scenarios.

We find abundant brGMGTs, which appear predominantly produced in the marine realm at the study site. Their abundance increases during the PETM, likely due to sea level rise and perhaps due to warming and a drop in seawater oxygen concentrations. Although speculative, an increase in brGMGT methylation during the PETM may be a

811 function of temperature, but a relation between brGMGT distribution and
812 environmental parameters including temperature is yet to be confirmed.
813

6. Data Availability

All data is provided in the Supplement Table and will be included in the PANGAEA database upon publication of this paper.

7. Sample Availability

Requests for materials can be addressed to A.Sluijs@uu.nl

8. Author Contributions

AS initiated the study, KGJN generated the data, JF modeled terrestrial contributions of isoGDGTs based on published information and the new Crenarchaeol data of the modern peat dataset, which was contributed by GNI. All authors contributed to the interpretation of the data and AS wrote the paper with input from all authors.

9. Competing Interests

The authors declare no competing interests

10. Acknowledgments

We thank the ACEX scientific party for collaborations over the past 16 years, the International Ocean Discovery Program (IODP) for access to ACEX samples and data, and the Dutch Research Council (NWO) for their continued support to IODP. We thank Linda van Roij for analytical support, Emily Dearing Crampton-Flood for providing BayMBT results and David Naafs for providing the original chromatograms published in Naafs et al. (2018b).

This research was funded by European Research Council Consolidator Grant 771497 awarded to AS and the Netherlands Earth System Science Centre, funded through a

839 Gravitation Grant by the Netherlands Ministry of Education, Culture and Science and
840 NWO. GNI acknowledges a GCRF Royal Society Dorothy Hodgkin Fellowship and
841 thanks.

842

843 **11. References**

844 Backman, J., Moran, K., McInroy, D. B., Mayer, L. A., and Expedition-302-Scientists:
845 Proceedings of the Integrated Ocean Drilling Program, 302, Integrated Ocean
846 Drilling Program Management International, Inc., Edinburgh, 2006.
847 Baxter, A. J., Hopmans, E. C., Russell, J. M., and Sinninghe Damsté, J. S.: Bacterial
848 GMGTs in East African lake sediments: Their potential as palaeotemperature
849 indicators, Geochim Cosmochim Ac, 259, 155-169,
850 https://doi.org/10.1016/j.gca.2019.05.039, 2019.
851 Berry, E. W.: A Possible Explanation of Upper Eocene Climates, Proceedings of the
852 American Philosophical Society, 61, 1-14, 1922.
853 Besseling, M. A., Hopmans, E. C., Bale, N. J., Schouten, S., Damsté, J. S. S., and
854 Villanueva, L.: The absence of intact polar lipid-derived GDGTs in marine waters
855 dominated by Marine Group II: Implications for lipid biosynthesis in Archaea,
856 Scientific Reports, 10, 294, 10.1038/s41598-019-57035-0, 2020.
857 Bijl, P. K., Schouten, S., Sluijs, A., Reichart, G.-J., Zachos, J. C., and Brinkhuis, H.:
858 Early Palaeogene temperature evolution of the southwest Pacific Ocean, Nature,
859 461, 776-779, 2009.
860 Bijl, P. K., Bendle, J. A. P., Bohaty, S. M., Pross, J., Schouten, S., Tauxe, L., Stickley,
861 C. E., McKay, R. M., Rohl, U., Olney, M., Sluijs, A., Escutia, C., Brinkhuis, H.,
862 and the Expedition 318 Scientists: Eocene cooling linked to early flow across the
863 Tasmanian Gateway, Proceedings of the National Academy of Sciences, 110,
864 9645-9650, 10.1073/pnas.1220872110, 2013.
865 Blaga, C. I., Reichart, G.-J., Heiri, O., and Sinninghe Damsté, J. S.: Tetraether
866 membrane lipid distributions in water-column particulate matter and sediments: a
867 study of 47 European lakes along a north–south transect, Journal of
868 Paleolimnology, 41, 523-540, 10.1007/s10933-008-9242-2, 2009.
869 Carton, J. A., Ding, Y., and Arrigo, K. R.: The seasonal cycle of the Arctic Ocean under
870 climate change, Geophysical Research Letters, 42, 7681-7686,
871 doi:10.1002/2015GL064514, 2015.
872 Chepurin, G. A., and Carton, J. A.: Subarctic and Arctic sea surface temperature and its
873 relation to ocean heat content 1982–2010, Journal of Geophysical Research:
874 Oceans, 117, doi:10.1029/2011JC007770, 2012.
875 Coolen, M. J. L., Abbas, B., Bleijswijk, J. v., Hopmans, E. C., Kuypers, M. M. M.,
876 Wakeham, S. G., and Damsté, J. S. S.: Putative ammonia-oxidizing Crenarchaeota
877 in suboxic waters of the Black Sea: a basin-wide ecological study using 16S
878 ribosomal and functional genes and membrane lipids, Environ Microbiol, 9, 1001-
879 1016, 2007.
880 Cramwinckel, M. J., Huber, M., Kocken, I. J., Agnini, C., Bijl, P. K., Bohaty, S. M.,
881 Frieling, J., Goldner, A., Hilgen, F. J., Kip, E. L., Peterse, F., van der Ploeg, R.,
882 Röhl, U., Schouten, S., and Sluijs, A.: Synchronous tropical and polar temperature
883 evolution in the Eocene, Nature, 559, 382-386, 10.1038/s41586-018-0272-2, 2018.

884 Cui, Y., Kump, L. R., Ridgwell, A. J., Charles, A. J., Junium, C. K., Diefendorf, A. F.,
885 Freeman, K. H., Urban, N. M., and Harding, I. C.: Slow release of fossil carbon
886 during the Palaeocene-Eocene Thermal Maximum, Nature Geoscience, 4, 481-485,
887 2011.
888 Dawson, M. R., West, R. M., Langston Jr, W., and Hutchison, J. H.: Paleogene
889 terrestrial vertebrates: Northernmost occurrence, Ellesmere Island, Canada,
890 Science, 192, 781-782, 1976.
891 De Jonge, C., Hopmans, E. C., Zell, C. I., Kim, J.-H., Schouten, S., and Sinninghe
892 Damsté, J. S.: Occurrence and abundance of 6-methyl branched glycerol dialkyl
893 glycerol tetraethers in soils: Implications for palaeoclimate reconstruction,
894 Geochim Cosmochim Ac, 141, 97-112, https://doi.org/10.1016/j.gca.2014.06.013,
895 2014.
896 De Jonge, C., Radujković, D., Sigurdsson, B. D., Weedon, J. T., Janssens, I., and
897 Peterse, F.: Lipid biomarker temperature proxy responds to abrupt shift in the
898 bacterial community composition in geothermally heated soils, Org Geochem, 137,
899 103897, https://doi.org/10.1016/j.orggeochem.2019.07.006, 2019.
900 De Rosa, M., Esposito, E., Gambacorta, A., Nicolaus, B., and Bu'Lock, J. D.: Effects
901 of temperature on ether lipid composition of Caldariella acidophila,
902 Phytochemistry, 19, 827-831, https://doi.org/10.1016/0031-9422(80)85120-X,
903 1980.
904 Dearing Crampton-Flood, E., Peterse, F., Munsterman, D., and Sinninghe Damsté, J.
905 S.: Using tetraether lipids archived in North Sea Basin sediments to extract North
906 Western European Pliocene continental air temperatures, Earth and Planetary
907 Science Letters, 490, 193-205, https://doi.org/10.1016/j.epsl.2018.03.030, 2018.
908 Dearing Crampton-Flood, E., Tierney, J. E., Peterse, F., Kirkels, F. M. S. A., and
909 Sinninghe Damsté, J. S.: BayMBT: A Bayesian calibration model for branched
910 glycerol dialkyl glycerol tetraethers in soils and peats, Geochim Cosmochim Ac,
911 268, 142-159, https://doi.org/10.1016/j.gca.2019.09.043, 2020.
912 Dong, L., Li, Z., and Jia, G.: Archaeal ammonia oxidation plays a part in late
913 Quaternary nitrogen cycling in the South China Sea, Earth and Planetary Science
914 Letters, 509, 38-46, https://doi.org/10.1016/j.epsl.2018.12.023, 2019.
915 Douglas, P. M. J., Affek, H. P., Ivany, L. C., Houben, A. J. P., Sijp, W. P., Sluijs, A.,
916 Schouten, S., and Pagani, M.: Pronounced zonal heterogeneity in Eocene southern
917 high-latitude sea surface temperatures, Proceedings of the National Academy of
918 Sciences of the United States of America, 111, 6582-6587, 2014.
919 Eberle, J. J., and Greenwood, D. R.: Life at the top of the greenhouse Eocene world—
920 A review of the Eocene flora and vertebrate fauna from Canada's High Arctic,
921 GSA Bulletin, 124, 3-23, 10.1130/B30571.1, 2012.
922 Elling, F. J., Könneke, M., Lipp, J. S., Becker, K. W., Gagen, E. J., and Hinrichs, K.-
923 U.: Effects of growth phase on the membrane lipid composition of the
924 thaumarchaeon Nitrosopumilus maritimus and their implications for archaeal lipid
925 distributions in the marine environment, Geochim Cosmochim Ac, 141, 579-597,
926 https://doi.org/10.1016/j.gca.2014.07.005, 2014.
927 Elling, F. J., Könneke, M., Mußmann, M., Greve, A., and Hinrichs, K.-U.: Influence of
928 temperature, pH, and salinity on membrane lipid composition and TEX86 of
929 marine planktonic thaumarchaeal isolates, Geochim Cosmochim Ac, 171, 238-255,
930 https://doi.org/10.1016/j.gca.2015.09.004, 2015.
931 Estes, R., and Hutchinson, J. H.: Eocene Lower Vertebrates from Ellesmere Island,
932 Canadian Arctic Archipelago, Palaeogeography, Palaeoclimatology,
933 Palaeoecology, 30, 325-347, 1980.

Evans, D., Sagoo, N., Renema, W., Cotton, L. J., Müller, W., Todd, J. A., Saraswati, P. K., Stassen, P., Ziegler, M., Pearson, P. N., Valdes, P. J., and Affek, H. P.: Eocene greenhouse climate revealed by coupled clumped isotope-Mg/Ca thermometry, Proceedings of the National Academy of Sciences, 115, 1174-1179, 10.1073/pnas.1714744115, 2018.

Frieling, J., Iakovleva, A. I., Reichart, G. J., Aleksandrova, G. N., Gnibidenko, Z. N., Schouten, S., and Sluijs, A.: Paleocene-Eocene warming and biotic response in the epicontinental West Siberian Sea, Geology, 42, 767-770, 2014.

Frieling, J., Gebhardt, H., Huber, M., Adekeye, O. A., Akande, S. O., Reichart, G.-J., Middelburg, J. J., Schouten, S., and Sluijs, A.: Extreme warmth and heat-stressed plankton in the tropics during the Paleocene-Eocene Thermal Maximum, Science Advances, 3, e1600891, 10.1126/sciadv.1600891, 2017.

Frieling, J., and Sluijs, A.: Towards quantitative environmental reconstructions from ancient non-analogue microfossil assemblages: Ecological preferences of Paleocene – Eocene dinoflagellates, Earth-Science Reviews, 185, 956-973, https://doi.org/10.1016/j.earscirev.2018.08.014, 2018.

Greenwood, D. R., and Wing, S. L.: Eocene continental climates and latitudinal temperature gradients, Geology, 23, 1044-1048, 1995.

Greenwood, D. R., Basinger, J. F., and Smith, R. Y.: How wet was the Arctic Eocene rain forest? Estimates of precipitation from Paleogene Arctic macrofloras, Geology, 38, 15-18, 10.1130/G30218.1, 2010.

Harding, I. C., Charles, A. J., Marshall, J. E. A., Pälike, H., Roberts, A. P., Wilson, P. A., Jarvis, E., Thorne, R., Morris, E., Moremon, R., Pearce, R. B., and Akbari, S.: Sea-level and salinity fluctuations during the Paleocene-Eocene thermal maximum in Arctic Spitsbergen, Earth and Planetary Science Letters, 303, 97-107, 2011.

Heer, O.: Flora fossilis Arctica, Kongliga Swenska Wetenskaps Academiens Handlingar, 4, Stockholm, Sweden, 41 pp., 1869.

Ho, S. L., Mollenhauer, G., Fietz, S., Martínez-Garcia, A., Lamy, F., Rueda, G., Schipper, K., Méheust, M., Rosell-Melé, A., Stein, R., and Tiedemann, R.: Appraisal of TEX86 and TEX86L thermometries in subpolar and polar regions, Geochim Cosmochim Ac, 131, 213-226, https://doi.org/10.1016/j.gca.2014.01.001, 2014.

Ho, S. L., and Laepple, T.: Flat meridional temperature gradient in the early Eocene in the subsurface rather than surface ocean, Nature Geoscience, 9, 606-610, 10.1038/ngeo2763.http://www.nature.com/ngeo/journal/v9/n8/abs/ngeo2763.html#supplementary-information, 2016.

Hollis, C. J., Dunkley Jones, T., Anagnostou, E., Bijl, P. K., Cramwinckel, M. J., Cui, Y., Dickens, G. R., Edgar, K. M., Eley, Y., Evans, D., Foster, G. L., Frieling, J., Inglis, G. N., Kennedy, E. M., Kozdon, R., Lauretano, V., Lear, C. H., Littler, K., Lourens, L., Meckler, A. N., Naafs, B. D. A., Pälike, H., Pancost, R. D., Pearson, P. N., Röhl, U., Royer, D. L., Salzmann, U., Schubert, B. A., Seebeck, H., Sluijs, A., Speijer, R. P., Stassen, P., Tierney, J., Tripati, A., Wade, B., Westerhold, T., Witkowski, C., Zachos, J. C., Zhang, Y. G., Huber, M., and Lunt, D. J.: The DeepMIP contribution to PMIP4: methodologies for selection, compilation and analysis of latest Paleocene and early Eocene climate proxy data, incorporating version 0.1 of the DeepMIP database, Geosci. Model Dev., 12, 3149-3206, 10.5194/gmd-12-3149-2019, 2019.

Hopmans, E. C., Schouten, S., Pancost, R. D., Meer, M. T. J. v. d., and Damsté, J. S. S.: Analysis of intact tetraether lipids in archaeal cell material and sediments by high performance liquid chromatography/atmospheric pressure chemical

ionization mass spectrometry, Rapid Communications in Mass Spectrometry, 14, 585-589, 2000.
Hopmans, E. C., Weijers, J. W. H., Schefuß, E., Herfort, L., Sinninghe Damsté, J. S., and Schouten, S.: A novel proxy for terrestrial organic matter in sediments based on branched and isoprenoid tetraether lipids, Earth and Planetary Science Letters, 224, 107-116, 2004.
Hopmans, E. C., Schouten, S., and Sinninghe Damsté, J. S.: The effect of improved chromatography on GDGT-based palaeoproxies, Org Geochem, 93, 1-6, https://doi.org/10.1016/j.orggeochem.2015.12.006, 2016.
Hurley, S. J., Elling, F. J., Könneke, M., Buchwald, C., Wankel, S. D., Santoro, A. E., Lipp, J. S., Hinrichs, K.-U., and Pearson, A.: Influence of ammonia oxidation rate on thaumarchaeal lipid composition and the TEX_{86} temperature proxy, Proceedings of the National Academy of Sciences, 113, 7762-7767, 10.1073/pnas.1518534113, 2016.
Inglis, G. N., Farnsworth, A., Lunt, D., Foster, G. L., Hollis, C. J., Pagani, M., Jardine, P. E., Pearson, P. N., Markwick, P., Galsworthy, A. M. J., Raynham, L., Taylor, K. W. R., and Pancost, R. D.: Descent toward the Icehouse: Eocene sea surface cooling inferred from GDGT distributions, Paleoceanography, 30, 1000-1020, 10.1002/2014PA002723, 2015.
Inglis, G. N., Farnsworth, A., Collinson, M. E., Carmichael, M. J., Naafs, B. D. A., Lunt, D. J., Valdes, P. J., and Pancost, R. D.: Terrestrial environmental change across the onset of the PETM and the associated impact on biomarker proxies: A cautionary tale, Global and Planetary Change, 181, 102991, https://doi.org/10.1016/j.gloplacha.2019.102991, 2019.
Jaeschke, A., Jørgensen, S. L., Bernasconi, S. M., Pedersen, R. B., Thorseth, I. H., and Früh-Green, G. L.: Microbial diversity of Loki's Castle black smokers at the Arctic Mid-Ocean Ridge, Geobiology, 10, 548-561, 10.1111/gbi.12009, 2012
Karner, M. B., DeLong, E. F., and Karl, D. M.: Archaeal dominance in the mesopelagic zone of the Pacific Ocean, Nature, 409, 507-510, 10.1038/35054051, 2001.
Kim, J.-H., Schouten, S., Hopmans, E. C., Donner, B., and Sinninghe Damste, J. S.: Global sediment core-top calibration of the TEX86 paleothermometer in the ocean, Geochim Cosmochim Ac, 72, 1154-1173, 2008.
Kim, J.-H., van der Meer, J., Schouten, S., Helmke, P., Willmott, V., Sangiorgi, F., Koç, N., Hopmans, E. C., and Sinninghe Damsté, J. S.: New indices and calibrations derived from the distribution of crenarchaeal isoprenoid tetraether lipids: Implications for past sea surface temperature reconstructions, Geochim Cosmochim Ac, 74, 4639-4654, 2010.
Kim, J.-H., Schouten, S., Rodrigo-Gámiz, M., Rampen, S., Marino, G., Huguet, C., Helmke, P., Buscail, R., Hopmans, E. C., Pross, J., Sangiorgi, F., Middelburg, J. B. M., and Sinninghe Damsté, J. S.: Influence of deep-water derived isoprenoid tetraether lipids on the paleothermometer in the Mediterranean Sea, Geochim Cosmochim Ac, 150, 125-141, http://dx.doi.org/10.1016/j.gca.2014.11.017, 2015.
Kirkels, F. M. S. A., Ponton, C., Galy, V., West, A. J., Feakins, S. J., and Peterse, F.: From Andes to Amazon: Assessing Branched Tetraether Lipids as Tracers for Soil Organic Carbon in the Madre de Dios River System, Journal of Geophysical Research: Biogeosciences, 125, e2019JG005270, 10.1029/2019jg005270, 2020.
Knies, J., Mann, U., Popp, B. N., Stein, R., and Brumsack, H.-J.: Surface water productivity and paleoceanographic implications in the Cenozoic Arctic Ocean, Paleoceanography, 23, PA1S16, 10.1029/2007pa001455, 2008.

Könneke, M., Bernhard, A. E., de la Torre, J. R., Walker, C. B., Waterbury, J. B., and Stahl, D. A.: Isolation of an autotrophic ammonia-oxidizing marine archaeon, Nature, 437, 543-546, 10.1038/nature03911, 2005.

Liu, X.-L., Summons, R. E., and Hinrichs, K.-U.: Extending the known range of glycerol ether lipids in the environment: structural assignments based on tandem mass spectral fragmentation patterns, Rapid Communications in Mass Spectrometry, 26, 2295-2302, 10.1002/rcm.6355, 2012.

Liu, Z., Pagani, M., Zinniker, D., DeConto, R., Huber, M., Brinkhuis, H., Shah, S. R., Leckie, R. M., and Pearson, A.: Global Cooling During the Eocene-Oligocene Climate Transition, Science, 323, 1187-1190, 10.1126/science.1166368, 2009.

Lunt, D. J., Jones, T. D., Heinemann, M., Huber, M., LeGrande, A., Winguth, A., Loptson, C., Marotzke, J., Roberts, C. D., Tindall, J., Valdes, P., and Winguth, C.: A model–data comparison for a multi-model ensemble of early Eocene atmosphere–ocean simulations: EoMIP, Climate of the Past, 8, 1717-1736, 2012.

März, C., Schnetger, B., and Brumsack, H. J.: Paleoenvironmental implications of Cenozoic sediments from the central Arctic Ocean (IODP Expedition 302) using inorganic geochemistry, Paleoceanography, 25, PA3206, 10.1029/2009pa001860, 2010.

Menzel, D., Hopmans, E. C., Schouten, S., and Sinninghe Damsté, J. S.: Membrane tetraether lipids of planktonic Crenarchaeota in Pliocene sapropels of the eastern Mediterranean Sea, Palaeogeography, Palaeoclimatology, Palaeoecology, 239, 1-15, 2006.

Mollenhauer, G., Basse, A., Kim, J.-H., Sinninghe Damsté, J. S., and Fischer, G.: A four-year record of UK'_{37}- and TEX86-derived sea surface temperature estimates from sinking particles in the filamentous upwelling region off Cape Blanc, Mauritania, Deep Sea Research Part I: Oceanographic Research Papers, 97, 67-79, https://doi.org/10.1016/j.dsr.2014.11.015, 2015.

Morales, C., Rogov, M., Wierzbowski, H., Ershova, V., Suan, G., Adatte, T., Föllmi, K. B., Tegelaar, E., Reichart, G.-J., de Lange, G. J., Middelburg, J. J., and van de Schootbrugge, B.: Glendonites track methane seepage in Mesozoic polar seas, Geology, 45, 503-506, 10.1130/g38967.1, 2017.

Müller, R. D., Cannon, J., Qin, X., Watson, R. J., Gurnis, M., Williams, S., Pfaffelmoser, T., Seton, M., Russell, S. H. J., and Zahirovic, S.: GPlates: Building a Virtual Earth Through Deep Time, Geochemistry, Geophysics, Geosystems, 19, 2243-2261, 10.1029/2018gc007584, 2018

Naafs, B. D. A., Inglis, G. N., Zheng, Y., Amesbury, M. J., Biester, H., Bindler, R., Blewett, J., Burrows, M. A., del Castillo Torres, D., Chambers, F. M., Cohen, A. D., Evershed, R. P., Feakins, S. J., Gałka, M., Gallego-Sala, A., Gandois, L., Gray, D. M., Hatcher, P. G., Honorio Coronado, E. N., Hughes, P. D. M., Huguet, A., Könönen, M., Laggoun-Défarge, F., Lähteenoja, O., Lamentowicz, M., Marchant, R., McClymont, E., Pontevedra-Pombal, X., Ponton, C., Pourmand, A., Rizzuti, A. M., Rochefort, L., Schellekens, J., De Vleeschouwer, F., and Pancost, R. D.: Introducing global peat-specific temperature and pH calibrations based on brGDGT bacterial lipids, Geochim Cosmochim Ac, 208, 285-301, https://doi.org/10.1016/j.gca.2017.01.038, 2017.

Naafs, B. D. A., McCormick, D., Inglis, G. N., and Pancost, R. D.: Archaeal and bacterial H-GDGTs are abundant in peat and their relative abundance is positively correlated with temperature, Geochim Cosmochim Ac, 227, 156-170, https://doi.org/10.1016/j.gca.2018.02.025, 2018a.

Naafs, B. D. A., Rohrssen, M., Inglis, G. N., Lähteenoja, O., Feakins, S. J., Collinson, M. E., Kennedy, E. M., Singh, P. K., Singh, M. P., Lunt, D. J., and Pancost, R. D.: High temperatures in the terrestrial mid-latitudes during the early Palaeogene, Nature Geoscience, 11, 766-771, 10.1038/s41561-018-0199-0, 2018b.

O'Brien, C. L., Robinson, S. A., Pancost, R. D., Sinninghe Damsté, J. S., Schouten, S., Lunt, D. J., Alsenz, H., Bornemann, A., Bottini, C., Brassell, S. C., Farnsworth, A., Forster, A., Huber, B. T., Inglis, G. N., Jenkyns, H. C., Linnert, C., Littler, K., Markwick, P., McAnena, A., Mutterlose, J., Naafs, B. D. A., Püttmann, W., Sluijs, A., van Helmond, N. A. G. M., Vellekoop, J., Wagner, T., and Wrobel, N. E.: Cretaceous sea-surface temperature evolution: Constraints from TEX86 and planktonic foraminiferal oxygen isotopes, Earth-Science Reviews, 172, 224-247, https://doi.org/10.1016/j.earscirev.2017.07.012, 2017.

O'Regan, M., Moran, K., Sangiorgi, F., Brinkhuis, H., Backman, J., Jakobsson, M., Stickley, C. E., Koc, N., Brumsack, H., Willard, D., Pockalny, R., and Skelton, A.: Mid-Cenozoic Tectonic and Paleoenvironmental setting of the Central Arctic Ocean, Paleoceanography, 23, PA1S20, doi:10.1029/2007PA001559, 2008.

Pagani, M., Pedentchouk, N., Huber, M., Sluijs, A., Schouten, S., Brinkhuis, H., Sinninghe Damsté, J. S., Dickens, G. R., and Expedition 302 Scientists, T.: Arctic hydrology during global warming at the Palaeocene-Eocene thermal maximum, Nature, 442, 671-675, 2006.

Pancost, R. D., Hopmans, E.C. and Sinninghe Damsté, J.S.: Archaeal lipids in mediterranean cold seeps: Molecular proxies for anaerobic methane oxidation. Geochimica et Cosmochimica Acta 65: 1611-1627, 2001.

Park, E., Hefter, J., Fischer, G., Iversen, M. H., Ramondenc, S., Nöthig, E. M., and Mollenhauer, G.: Seasonality of archaeal lipid flux and GDGT-based thermometry in sinking particles of high-latitude oceans: Fram Strait (79°N) and Antarctic Polar Front (50°S), Biogeosciences, 16, 2247-2268, 10.5194/bg-16-2247-2019, 2019.

Pierrehumbert, R. T.: The hydrologic cycle in deep-time climate problems, Nature, 419, 191-198, 2002.

Pitcher, A., Hopmans, E. C., Mosier, A. C., Park, S.-J., Rhee, S.-K., Francis, C. A., Schouten, S., and Sinninghe Damsté, J. S.: Core and Intact Polar Glycerol Dibiphytanyl Glycerol Tetraether Lipids of Ammonia-Oxidizing Archaea Enriched from Marine and Estuarine Sediments, Applied and Environmental Microbiology, 77, 3468-3477, 10.1128/aem.02758-10, 2011a.

Pitcher, A., Wuchter, C., Siedenberg, K., Schouten, S., and Sinninghe Damsté, J. S.: Crenarchaeol tracks winter blooms of ammonia-oxidizing Thaumarchaeota in the coastal North Sea, Limnol Oceanogr, 56, 2308-2318, 10.4319/lo.2011.56.6.2308, 2011b.

Qin, W., Amin, S. A., Martens-Habbena, W., Walker, C. B., Urakawa, H., Devol, A. H., Ingalls, A. E., Moffett, J. W., Armbrust, E. V., and Stahl, D. A.: Marine ammonia-oxidizing archaeal isolates display obligate mixotrophy and wide ecotypic variation, Proceedings of the National Academy of Sciences, 111, 12504-12509, 10.1073/pnas.1324115111, 2014.

Qin, W., Carlson, L. T., Armbrust, E. V., Devol, A. H., Moffett, J. W., Stahl, D. A., and Ingalls, A. E.: Confounding effects of oxygen and temperature on the TEX_{86} signature of marine Thaumarchaeota, Proceedings of the National Academy of Sciences, 112, 10979-10984, 10.1073/pnas.1501568112, 2015.

Reichgelt, T., West, C. K., and Greenwood, D. R.: The relation between global palm distribution and climate, Scientific Reports, 8, 4721, 10.1038/s41598-018-23147-2, 2018.

Richey, J. N., and Tierney, J. E.: GDGT and alkenone flux in the northern Gulf of Mexico: Implications for the TEX86 and UK'37 paleothermometers, Paleoceanography, 31, 1547-1561, 10.1002/2016pa003032, 2016.
Sangiorgi, F., van Soelen, E. E., Spofforth, D. J. A., Pälike, H., Stickley, C. E., St. John, K., Koç, N., Schouten, S., Sinninghe Damsté, J. S., and Brinkhuis, H.: Cyclicity in the middle Eocene central Arctic Ocean sediment record: Orbital forcing and environmental response, Paleoceanography, 23, n/a-n/a, 10.1029/2007PA001487, 2008.
Schouten, S., Hopmans, E. C., Schefuß, E., and Sinninghe Damsté, J. S.: Distributional variations in marine crenarchaeotal membrane lipids: a new tool for reconstructing ancient sea water temperatures?, Earth and Planetary Science Letters, 204, 265-274, 2002.
Schouten, S., Hopmans, E. C., Forster, A., Breugel, Y. V., Kuypers, M. M. M., and Sinninghe Damsté, J. S.: Extremely high sea-surface temperatures at low latitudes during the middle Cretaceous as revealed by archaeal membrane lipids, Geology, 31, 1069-1072, 2003.
Schouten, S., Forster, A., Panoto, F. E., and Sinninghe Damste, J. S.: Towards calibration of the TEX86 palaeothermometer for tropical sea surface temperatures in ancient greenhouse worlds, Org Geochem, 38, 1537-1546, 2007a.
Schouten, S., Baas, M., Hopmans, E. C., and Sinninghe Damsté, J. S.: An unusual isoprenoid tetraether lipid in marine and lacustrine sediments, Org Geochem, 39, 1033-1038, 2008.
Schouten, S., Hopmans, E. C., Meer, J. v. d., Mets, A., Bard, E., Bianchi, T. S., Diefendorf, A., Escala, M., Freeman, K. H., Furukawa, Y., Ingalls, C. H. a. A., Ménot-Combes, G., Nederbragt, A. J., Oba, M., Pearson, A., Pearson, E. J., Rosell-Melé, A., Schaeffer, P., Shah, S. R., Shanahan, T. M., Smith, R. W., Smittenberg, R., Talbot, H. M., Uchida, M., Mooy, B. A. S. V., Yamamoto, M., Zhang, Z., and Sinninghe Damsté, J. S.: An interlaboratory study of TEX86 and BIT analysis using high-performance liquid chromatography–mass spectrometry, Geochemistry Geophysics Geosystems, 10, Q03012, doi:03010.01029/02008GC002221, 2009.
Schouten, S., Hopmans, E. C., and Sinninghe Damsté, J. S.: The organic geochemistry of glycerol dialkyl glycerol tetraether lipids: A review, Org Geochem, 54, 19-61, http://dx.doi.org/10.1016/j.orggeochem.2012.09.006, 2013.
Schweitzer, H.-J.: Environment and climate in the early Tertiary of Spitsbergen, Palaeogeography, Palaeoclimatology, Palaeoecology, 30, 297-311, 1980.
Seton, M., Müller, R. D., Zahirovic, S., Gaina, C., Torsvik, T., Shephard, G., Talsma, A., Gurnis, M., Turner, M., Maus, S., and Chandler, M.: Global continental and ocean basin reconstructions since 200Ma, Earth-Science Reviews, 113, 212-270, https://doi.org/10.1016/j.earscirev.2012.03.002, 2012.
Shah, S. R., Mollenhauer, G., Ohkouchi, N., Eglinton, T. I., and Pearson, A.: Origins of archaeal tetraether lipids in sediments: Insights from radiocarbon analysis, Geochim Cosmochim Ac, 72, 4577-4594, https://doi.org/10.1016/j.gca.2008.06.021, 2008.
Sinninghe Damsté, J. S., Wakeham, S. G., Kohnen, M. E. L., Hayes, J. M., and de Leeuw, J. W.: A 6,000-year sedimentary molecular record of chemocline excursions in the Black Sea, Nature, 362, 827 - 829, 1993.
Sinninghe Damsté, J. S., Rijpstra, W. I. C., Hopmans, E. C., Weijers, J. W. H., Foesel, B. U., Overmann, J., and Dedysh, S. N.: 13,16-Dimethyl Octacosanedioic Acid (*iso*-Diabolic Acid), a Common Membrane-Spanning Lipid of Acidobacteria

Subdivisions 1 and 3, Applied and Environmental Microbiology, 77, 4147-4154, 10.1128/aem.00466-11, 2011.
Sinninghe Damsté, J. S.: Spatial heterogeneity of sources of branched tetraethers in shelf systems: The geochemistry of tetraethers in the Berau River delta (Kalimantan, Indonesia), Geochim Cosmochim Ac, 186, 13-31, https://doi.org/10.1016/j.gca.2016.04.033, 2016.
Sinninghe Damsté, J. S., Rijpstra, W. I. C., Foesel, B. U., Huber, K. J., Overmann, J., Nakagawa, S., Kim, J. J., Dunfield, P. F., Dedysh, S. N., and Villanueva, L.: An overview of the occurrence of ether- and ester-linked iso-diabolic acid membrane lipids in microbial cultures of the Acidobacteria: Implications for brGDGT paleoproxies for temperature and pH, Org Geochem, 124, 63-76, https://doi.org/10.1016/j.orggeochem.2018.07.006, 2018a.
Sinninghe Damsté, J. S., Rijpstra, W. I. C., Hopmans, E. C., den Uijl, M. J., Weijers, J. W. H., and Schouten, S.: The enigmatic structure of the crenarchaeol isomer, Org Geochem, 124, 22-28, https://doi.org/10.1016/j.orggeochem.2018.06.005, 2018b
Sluijs, A., Schouten, S., Pagani, M., Woltering, M., Brinkhuis, H., Sinninghe Damsté, J. S., Dickens, G. R., Huber, M., Reichart, G.-J., Stein, R., Matthiessen, J., Lourens, L. J., Pedentchouk, N., Backman, J., Moran, K., and The Expedition 302 Scientists: Subtropical Arctic Ocean temperatures during the Palaeocene/Eocene thermal maximum, Nature, 441, 610-613, 2006.
Sluijs, A., Brinkhuis, H., Crouch, E. M., John, C. M., Handley, L., Munsterman, D., Bohaty, S., M., Zachos, J. C., Reichart, G.-J., Schouten, S., Pancost, R. D., Sinninghe Damsté, J. S., Welters, N. L. D., Lotter, A. F., and Dickens, G. R.: Eustatic variations during the Paleocene-Eocene greenhouse world, Paleoceanography, 23, PA4216, doi:10.1029/2008PA001615, 2008a.
Sluijs, A., Röhl, U., Schouten, S., Brumsack, H.-J., Sangiorgi, F., Sinninghe Damsté, J. S., and Brinkhuis, H.: Arctic late Paleocene–early Eocene paleoenvironments with special emphasis on the Paleocene-Eocene thermal maximum (Lomonosov Ridge, Integrated Ocean Drilling Program Expedition 302), Paleoceanography, 23, PA1S11, doi:10.1029/2007PA001495, 2008b.
Sluijs, A., Schouten, S., Donders, T. H., Schoon, P. L., Röhl, U., Reichart, G. J., Sangiorgi, F., Kim, J.-H., Sinninghe Damsté, J. S., and Brinkhuis, H.: Warm and Wet Conditions in the Arctic Region during Eocene Thermal Maximum 2, Nature Geoscience, 2, 777-780, 2009.
Sluijs, A., and Dickens, G. R.: Assessing offsets between the δ13C of sedimentary components and the global exogenic carbon pool across Early Paleogene carbon cycle perturbations, Global Biogeochemical Cycles, 26, GB4005, doi:10.1029/2011GB004224, 2012.
Sollich, M., Yoshinaga, M. Y., Häusler, S., Price, R. E., Hinrichs, K.-U., and Bühring, S. I.: Heat Stress Dictates Microbial Lipid Composition along a Thermal Gradient in Marine Sediments, Frontiers in Microbiology, 8, 10.3389/fmicb.2017.01550, 2017.
Spielhagen, R. F., and Tripati, A.: Evidence from Svalbard for near-freezing temperatures and climate oscillations in the Arctic during the Paleocene and Eocene, Palaeogeography, Palaeoclimatology, Palaeoecology, 278, 48-56, https://doi.org/10.1016/j.palaeo.2009.04.012, 2009.
Stein, R., Boucsein, B., and Meyer, H.: Anoxia and high primary production in the Paleogene central Arctic Ocean: First detailed records from Lomonosov Ridge, Geophysical Research Letters, 33, L18606, doi:10.1029/2006GL026776, 2006.

Stein, R.: Upper Cretaceous/lower Tertiary black shales near the North Pole: Organic-carbon origin and source-rock potential, Marine and Petroleum Geology, 24, 67-73, 2007.
Suan, G., Popescu, S.-M., Yoon, D., Baudin, F., Suc, J.-P., Schnyder, J., Labrousse, L., Fauquette, S., Piepjohn, K., and Sobolev, N. N.: Subtropical climate conditions and mangrove growth in Arctic Siberia during the early Eocene, Geology, 45, 539-542, 10.1130/g38547.1, 2017.
Taylor, K. W. R., Huber, M., Hollis, C. J., Hernandez-Sanchez, M. T., and Pancost, R. D.: Re-evaluating modern and Palaeogene GDGT distributions: Implications for SST reconstructions, Global and Planetary Change, 108, 158-174, http://dx.doi.org/10.1016/j.gloplacha.2013.06.011, 2013.
Teichert, B. M. A., and Luppold, F. W.: Glendonites from an Early Jurassic methane seep — Climate or methane indicators?, Palaeogeography, Palaeoclimatology, Palaeoecology, 390, 81-93, https://doi.org/10.1016/j.palaeo.2013.03.001, 2013.
Tierney, J. E., and Tingley, M. P.: A Bayesian, spatially-varying calibration model for the TEX86 proxy, Geochim Cosmochim Ac, 127, 83-106, http://dx.doi.org/10.1016/j.gca.2013.11.026, 2014.
Tierney, J. E., Sinninghe Damsté, J. S., Pancost, R. D., Sluijs, A., and Zachos, J. C.: Eocene temperature gradients, Nature Geosci, 10, 538-539, 10.1038/ngeo2997, 2017.
Torsvik, T. H., Van der Voo, R., Preeden, U., Mac Niocaill, C., Steinberger, B., Doubrovine, P. V., van Hinsbergen, D. J. J., Domeier, M., Gaina, C., Tohver, E., Meert, J. G., McCausland, P. J. A., and Cocks, L. R. M.: Phanerozoic polar wander, palaeogeography and dynamics, Earth-Science Reviews, 114, 325-368, https://doi.org/10.1016/j.earscirev.2012.06.007, 2012.
Trommer, G., Siccha, M., van der Meer, M. T. J., Schouten, S., Sinninghe Damsté, J. S., Schulz, H., Hemleben, C., and Kucera, M.: Distribution of Crenarchaeota tetraether membrane lipids in surface sediments from the Red Sea, Org Geochem, 40, 724-731, https://doi.org/10.1016/j.orggeochem.2009.03.001, 2009.
Uhl, D., Traiser, C., Griesser, U., and Denk, T.: Fossil leaves as palaeoclimate proxies in the Palaeogene of Spitsbergen (Svalbard), Acta Palaeobotanica, 47, 89-107, 2007.
Van der Burgh, J.: Some palms in the Miocene of the lower Rhenish Plain, Review of Palaeobotany and Palynology, 40, 359-374, 1984.
Van Hinsbergen, D. J. J., de Groot, L. V., van Schaik, S. J., Spakman, W., Bijl, P. K., Sluijs, A., Langereis, C. G., and Brinkhuis, H.: A Paleolatitude Calculator for Paleoclimate Studies, PLOS ONE, 10, e0126946, 10.1371/journal.pone.0126946, 2015.
Wakeham, S. G., Amann, R., Freeman, K. H., Hopmans, E. C., Jörgensen, B. B., Putnam, I. F., Schouten, S., Sinninghe Damsté, J. S., Talbot, H. M., and Woebken, D.: Microbial ecology of the stratified water column of the Black Sea as revealed by a comprehensive biomarker stud, Org Geochem, 38, 2070-2097, 2007.
Weijers, J. W. H., Schouten, S., Spaargaren, O. C., and Sinninghe Damsté, J. S.: Occurrence and distribution of tetraether membrane lipids in soils: Implications for the use of the TEX86 proxy and the BIT index, Org Geochem, 37, 1680-1693, 2006.
Weijers, J. W. H., Schouten, S., Sluijs, A., Brinkhuis, H., and Sinninghe Damsté, J. S.: Warm arctic continents during the Palaeocene-Eocene thermal maximum, Earth and Planetary Science Letters, 261, 230-238, 2007a.

Weijers, J. W. H., Schouten, S., van den Donker, J. C., Hopmans, E. C., and Sinninghe Damsté, J. S.: Environmental controls on bacterial tetraether membrane lipid distribution in soils, Geochim Cosmochim Ac, 71, 703-713, 2007b.

Weijers, J. W. H., Lim, K. L. H., Aquilina, A., Sinninghe Damsté, J. S., and Pancost, R. D.: Biogeochemical controls on glycerol dialkyl glycerol tetraether lipid distributions in sediments characterized by diffusive methane flux, Geochemistry, Geophysics, Geosystems, 12, doi:10.1029/2011GC003724, 2011.

Willard, D. A., Donders, T. H., Reichgelt, T., Greenwood, D. R., Sangiorgi, F., Peterse, F., Nierop, K. G. J., Frieling, J., Schouten, S., and Sluijs, A.: Arctic vegetation, temperature, and hydrology during Early Eocene transient global warming events, Global and Planetary Change, 178, 139-152, https://doi.org/10.1016/j.gloplacha.2019.04.012, 2019.

Wuchter, C., Schouten, S., Coolen, M. J. L., and Sinninghe Damsté, J. S.: Temperature-dependent variation in the distribution of tetraether membrane lipids of marine Crenarchaeota: Implications for TEX86 paleothermometry, Paleoceanography, 19, PA402, 2004.

Wuchter, C., Schouten, S., Wakeham, S. G., and Sinninghe Damste, J. S.: Temporal and spatial variation in tetraether membrane lipids of marine Crenarchaeota in particulate organic matter: Implications for TEX86 paleothermometry, Paleoceanography, 20, doi:10.1029/2004PA001110, 2005.

Wuchter, C., Abbas, B., Coolen, M. J. L., Herfort, L., van Bleijswijk, J., Timmers, P., Strous, M., Teira, E., Herndl, G. J., Middelburg, J. J., Schouten, S., and Damste, J. S. S.: Archaeal nitrification in the ocean, Proceedings of the National Academy of Sciences of the United States of America, 103, 12317-12322, 10.1073/pnas.0600756103, 2006a.

Wuchter, C., Schouten, S., Wakeham, S. G., and Sinninghe Damsté, J. S.: Archaeal tetraether membrane lipid fluxes in the northeastern Pacific and the Arabian Sea: Implications for TEX86 paleothermometry, Paleoceanography, 21, PA4208, 2006b.

Xie, S., Liu, X.-L., Schubotz, F., Wakeham, S. G., and Hinrichs, K.-U.: Distribution of glycerol ether lipids in the oxygen minimum zone of the Eastern Tropical North Pacific Ocean, Org Geochem, 71, 60-71, https://doi.org/10.1016/j.orggeochem.2014.04.006, 2014.

Yamamoto, M., Shimamoto, A., Fukuhara, T., Tanaka, Y., and Ishizaka, J.: Glycerol dialkyl glycerol tetraethers and TEX86 index in sinking particles in the western North Pacific, Org Geochem, 53, 52-62, https://doi.org/10.1016/j.orggeochem.2012.04.010, 2012.

Zeng, Z., Liu, X.-L., Farley, K. R., Wei, J. H., Metcalf, W. W., Summons, R. E., and Welander, P. V.: GDGT cyclization proteins identify the dominant archaeal sources of tetraether lipids in the ocean, Proceedings of the National Academy of Sciences, 116, 22505-22511, 10.1073/pnas.1909306116, 2019.

Zhang, Y. G., Zhang, C. L., Liu, X.-L., Li, L., Hinrichs, K.-U., and Noakes, J. E.: Methane Index: A tetraether archaeal lipid biomarker indicator for detecting the instability of marine gas hydrates, Earth and Planetary Science Letters, 307, 525-534, https://doi.org/10.1016/j.epsl.2011.05.031, 2011.

Zhang, Y. G., Pagani, M., and Wang, Z.: Ring Index: A new strategy to evaluate the integrity of TEX86 paleothermometry, Paleoceanography, 31, 220-232, doi:10.1002/2015PA002848, 2016.

Zhang, Y. G., and Liu, X.: Export Depth of the TEX86 Signal, Paleoceanography and Paleoclimatology, 33, 666-671, 10.1029/2018pa003337, 2018.

Zhu, J., Poulsen, C. J., and Tierney, J. E.: Simulation of Eocene extreme warmth and high climate sensitivity through cloud feedbacks, Science Advances, 5, eaax1874, 10.1126/sciadv.aax1874, 2019.

Figure 1. Location of ACEX Hole 4A within a paleogeographic reconstruction of the Arctic region at the time of the PETM. Reconstruction made using gplates (Müller et al., 2018), with the tectonic reconstruction of Seton et al. (2012, red shape is Lomonosov Ridge in this reconstruction and grey lines are structural features including spreading ridges), the paleomagnetic reference frame of Torsvik et al., (2012), and modern coastlines.

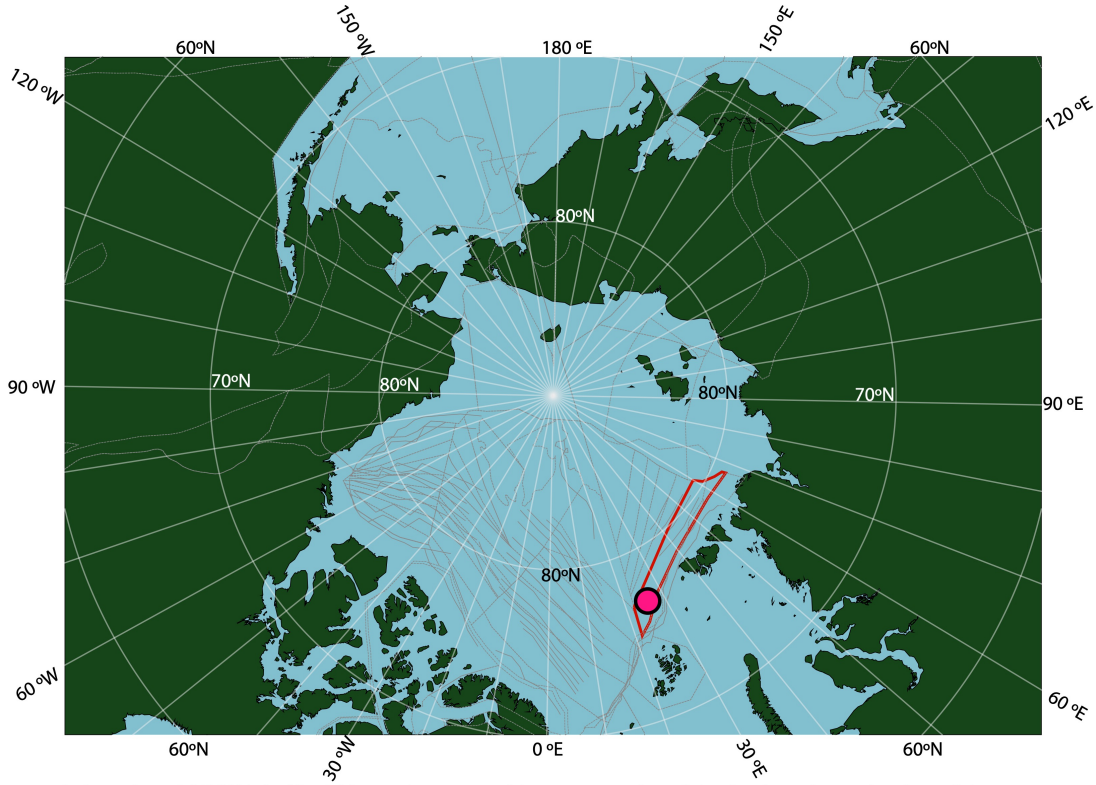

Figure 2. Molecular structures of the relevant isoGDGTs, brGDGTs and brGMGTs and their terminology as described in this study. Crenarchaeol isomer (not shown) differs from Crenarchaeol in the stereochemistry of the cyclopentane moiety adjacent to the cyclohexyl moiety (Sinninghe Damsté et al., 2018b). For the terminology of the brGMGTs, for which the exact chemical structure is still unclear, we follow Baxter et al. (2019), since we identify the same isomers (see Figure S2 for a chromatogram).

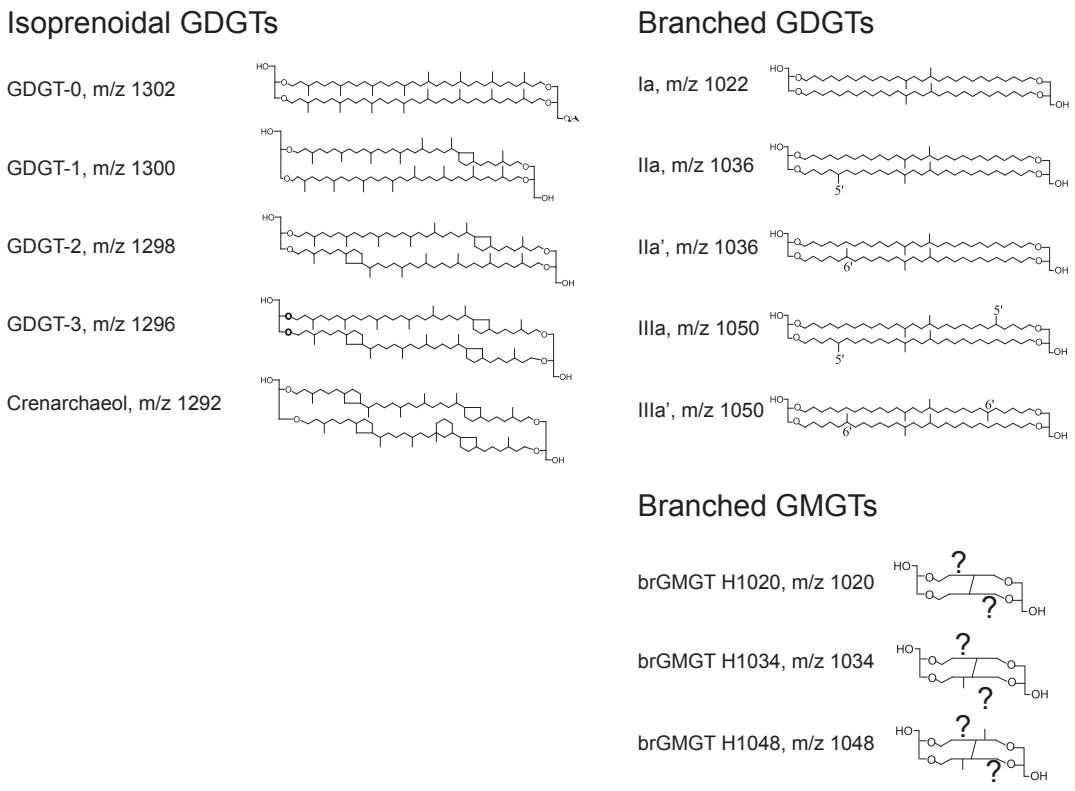

Figure 3. Comparison of the original GDGT dataset of the upper Paleocene and lower Eocene of ACEX Hole 4A (Sluijs et al., 2006; Sluijs et al., 2009) and the new data generated according to the latest chromatography protocols.

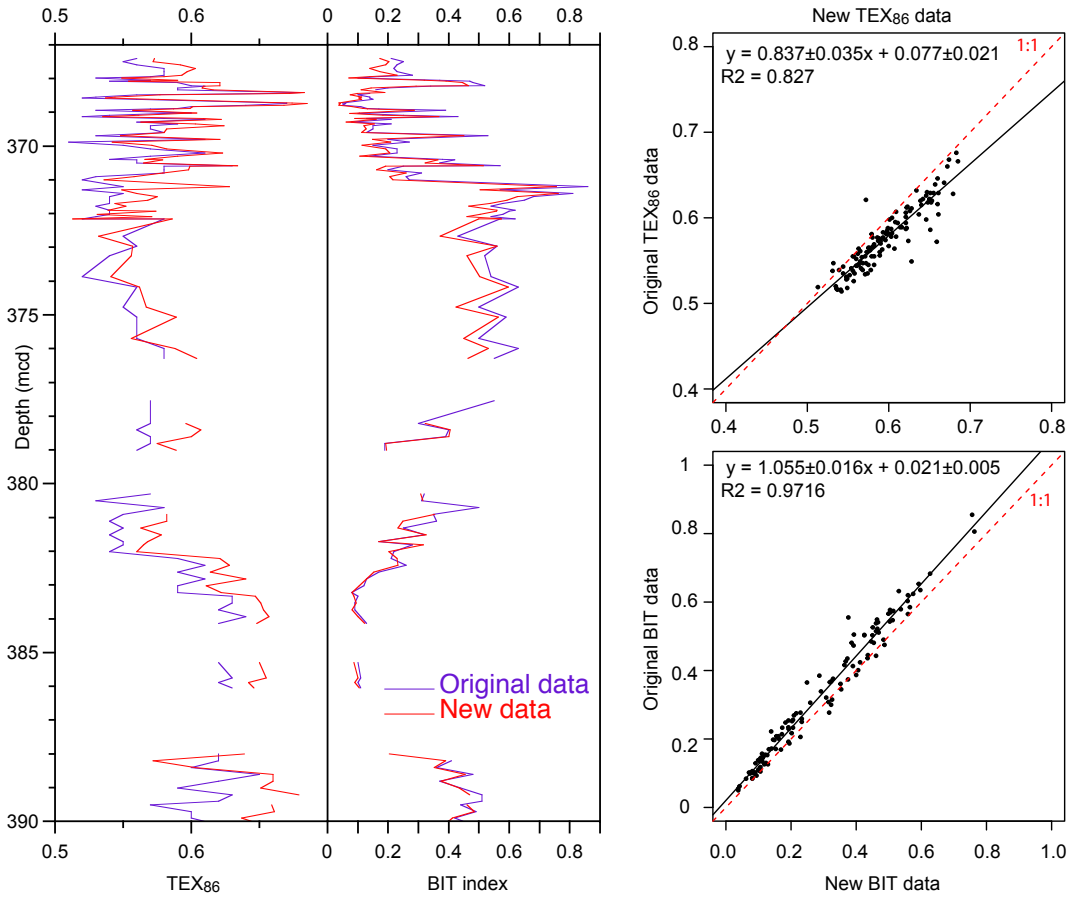

Figure 4. Comparison between BIT index values and TEX_{86} for various intervals spanning the upper Paleocene and lower Eocene of ACEX Hole 4A.

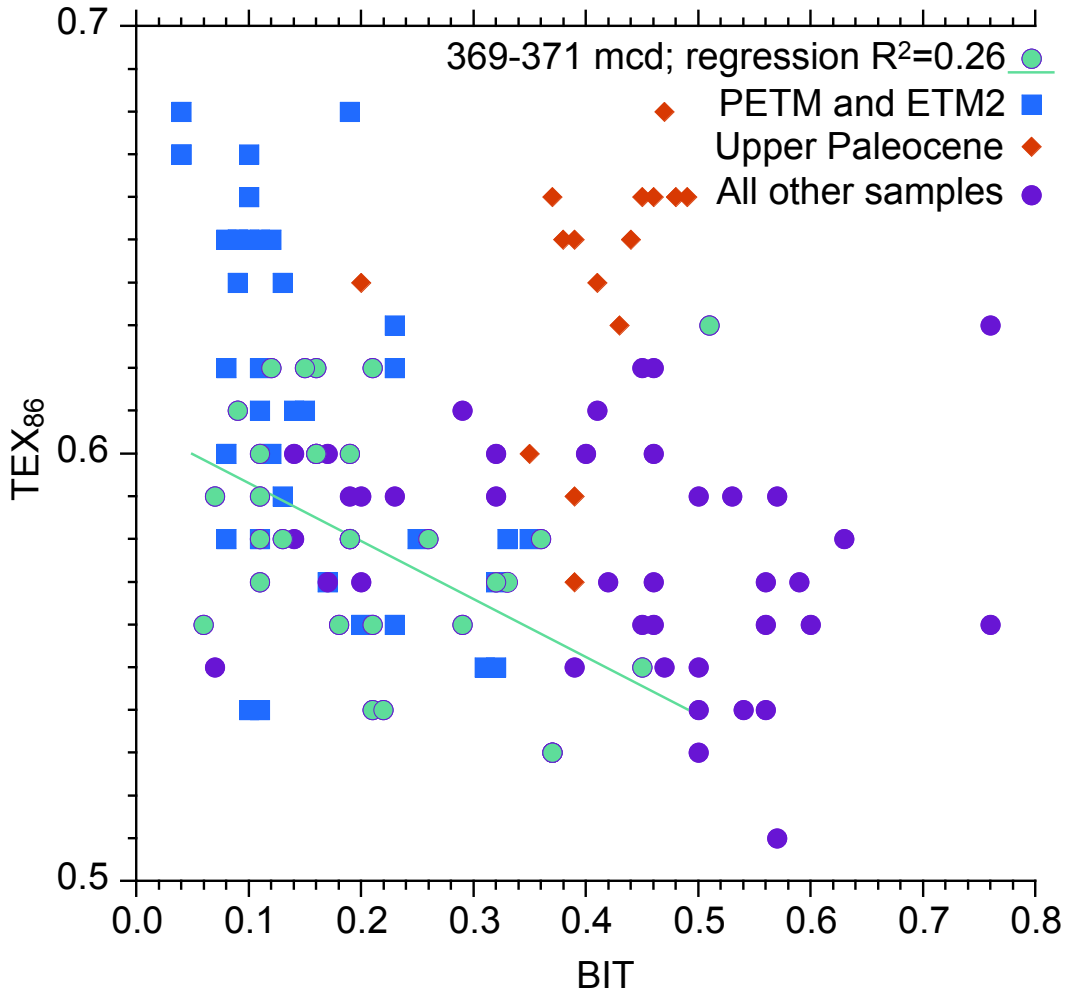

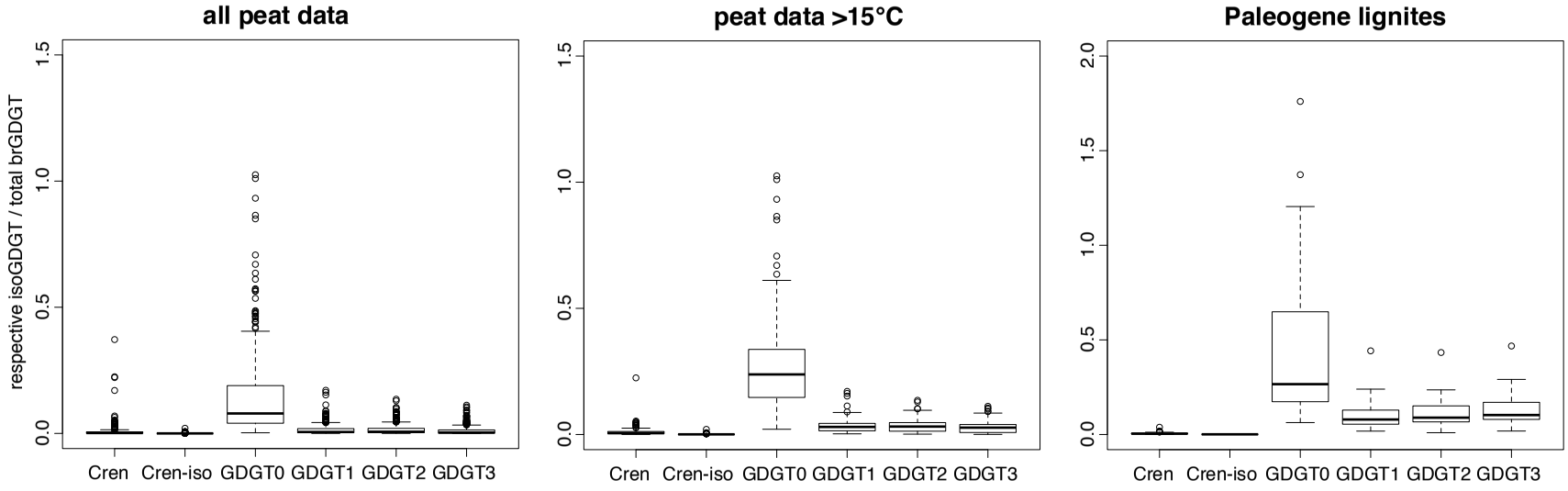

Figure 5. The abundance of various isoGDGTs relative to the total brGDGT abundance in modern peats (left 2 panels) and Paleogene lignites (right panel; Equation 9), used to assess potential isoGDGT contributions to the ACEX samples. The box is standard 25%-50%-75% quantiles, whiskers represent box limits plus/minus 1.5 x the interquartile range (IQR). Any data outside that range is given as circles. Number of measurements per dataset: Modern peats = 473 (most isoGDGTs have been identified in ±430 of those; Modern peats above 15ºC = 141 (all except one of there have isoGDGT data; Lignites = 58 (allof which have isoGDGT data but only 29 have available (quantifiable) crenarchaeol isomer data).

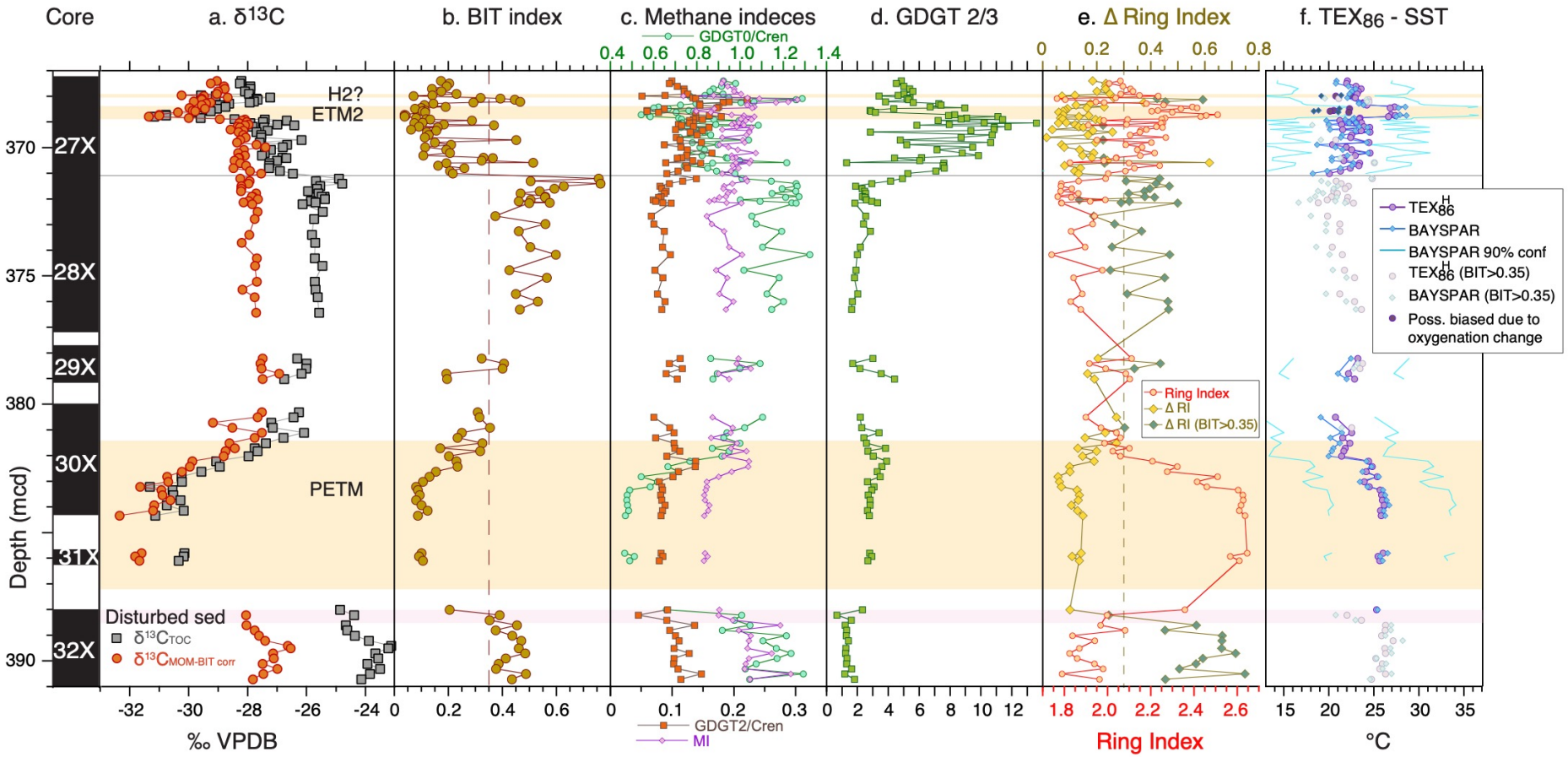

Figure 6. Branched and Isoprenoid GDGT records across the upper Paleocene and lower Eocene of ACEX Hole 4A. a. carbon isotope stratigraphy (total organic carbon record from Sluijs et al., 2006 and 2009; marine organic matter record from Sluijs and Dickens (2012)), b. BIT index (equation 2), c. indices indicative of anaerobic archaeal methanotrophy (MI index (equation 3) and GDGT-2/Crenarchaeol), and methanogenesis (GDGT-0/Crenarchaeol), d. GDGT2-GDGT3 ratio, e. Ring index (equation 5) and Δ Ring Index, f. TEX_{86} (equation 1) calibrated to sea surface temperature using a non-linear calibration TEX_{86}^{H} calibration (Kim et al., 2010) and the BAYSPAR method, which is based on a linear calibration (Tierney and Tingley, 2014).

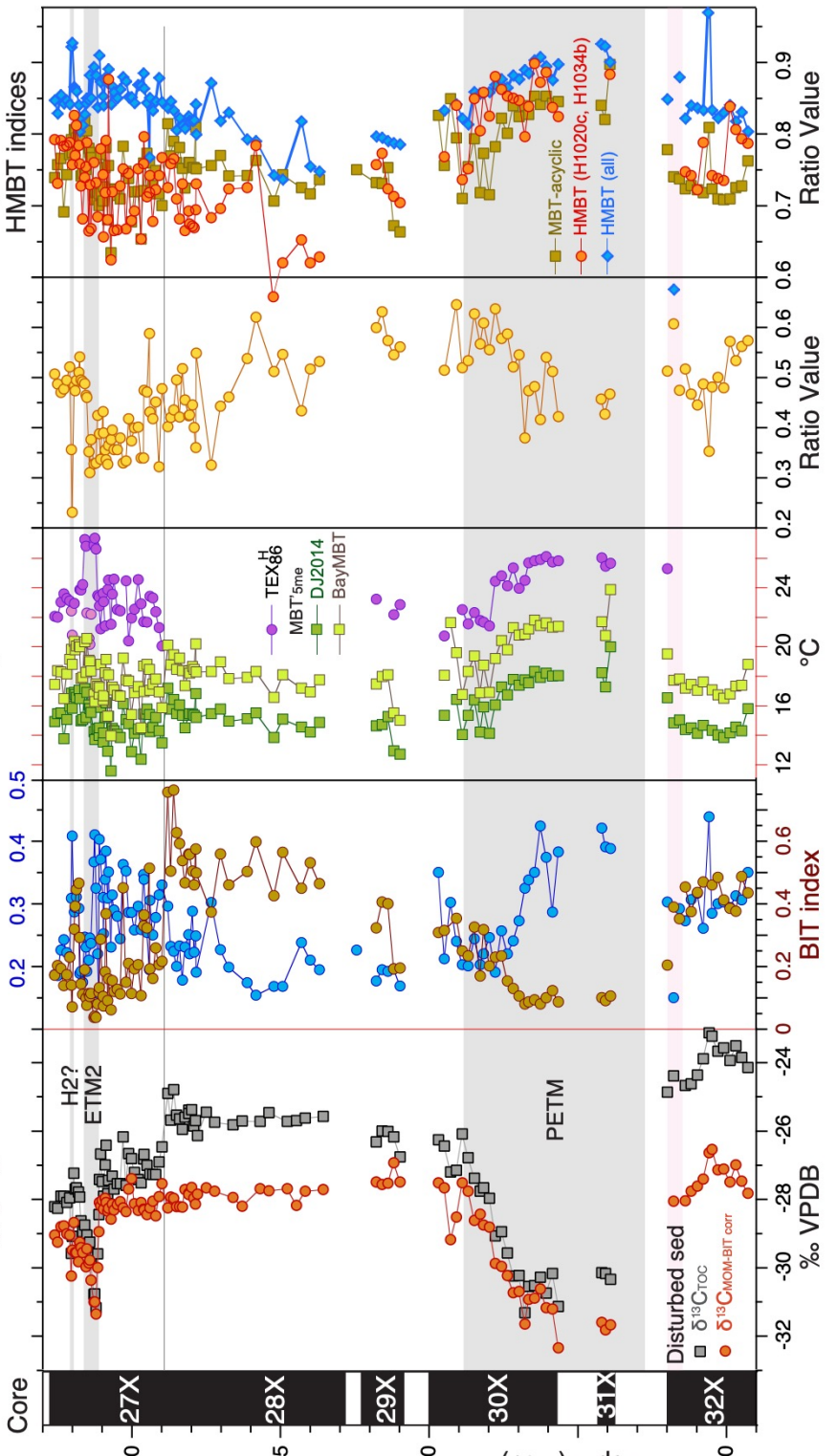

Figure 7. Branched GMGT records across the upper Paleocene and lower Eocene of ACEX Hole 4A. a. carbon isotope stratigraphy (total organic carbon record from Sluijs et al., 2006 and 2009; marine organic matter record from Sluijs and Dickens (2012)), b. fraction of brGMGTs of the total branched GDGTs and GMGTs and BIT index (equation 2), c. MBT'_{5me} record (Willard et al., 2019) using the calibrations of De Jonge et al. (2014) and BayMBT (Dearing Crampton-Flood, 2020; Median value; see Supplementary Table for uncertainty) and TEX_{86}^{H}, d. MBT*acyclic* (equation 6) and H-MBT based on all isomers detected with m/z 1020 and m/z 1034 (H-MBT all; equation 7) and based on H1020a and H1034b (H-MBT H1020a, H1034c), e. brGMGT-1 record (equation 8).